Master Thesis, Department of Geosciences

A noise model for shallow water North Sea

Deneke Admasu Fetene

UNIVERSITY OF OSLO

FACULTY OF MATHEMATICS AND NATURAL SCIENCES

A noise model for shallow water North Sea

Deneke Admasu Fetene

Master Thesis in Geosciences

Discipline: Geophysics

Department of Geosciences

Faculty of Mathematics and Natural Sciences

University of Oslo

June 2014

Acknowledgements

My supervisor Professor Leiv Jacob Gelius at the University of Oslo is greatly acknowledged for his decisive roles contributing in my course of study and particularly to this work.

I would like to thank Dr. Vetle Vinje Principal Geophysicist for advising and collaboration at CGG.

Also further thanks to Dr. Carl-Inge Colombo Nilsen for his assistance with some coding at CGG.

I would like also to thank Professor Valerie Maupin at the University of Oslo for advising and facilitating the collaboration with CGG at beginning of this work.

I owe a debt of gratitude to my family and friends for their constant and unflagging support and encouragement over the course of my study.

It is also my pleasure to thank the Geophysics groups at the University of Oslo, staff at the CGG and to all those who have in one way or another contributed to this work.

Most of all I would like to extol GOD incessantly for HIS dear help.

Oslo, June 2014

Deneke Admasu Fetene

Abstract

The purpose of this study is to improve the basic understanding of the propagating mechanisms behind seismic interference noise. A Matlab code of the normal mode solution in Pekeris waveguide model was developed and numerical simulations were done. The collection of data was examined carefully and a small subset was chosen for further analysis and comparison with numerical simulations. Comparison of the output from this modeling code in the far-field with real noise recordings in case of a slanted-streamer was performed.

From the simulations it is observed that the rate of dispersion, attenuation and the transmission loss depend on both mode number and range. For both simulated and real data it is observed that, following the dispersive character of the waveguide seen, the higher frequencies significantly more attenuated than the lower ones. It was also shown that the real noise recordings locally looked similar to the simulated data. Thus, indicating SI noise show close resemblance with dispersive modes. However, one main difference exists between simulated and recorded data; the latter has much longer time duration. The unknown representation of the position of the source and the inhomogeneity of the water column could be the possible reason for this difference.

Table of Contents

Contents

1. Introduction

1.1 Background and motivation

Marine seismic data are generated by sources placed at some depth in the water column and are registered by sensors placed along seismic streamers towed at some depth in the water column. However the records are often contaminated by guided waves that propagate horizontally within the water layer or in the layers beneath the water layer. This results in recordings that contain in addition to the signal, also undesired noise. This noise is coming from a number of sources; the sea surface, industrial activity, other seismic vessels, noise in the recording equipment, mammal noise etc.

The characteristics of the waves depend on water depth, on the geometry and material properties of the bottom layer. For instance the signal-to-noise ratio is a key characteristic of a seismic acquisition and high levels of noise is a limiting factor in imaging. Therefore modeling of the propagation of such pressure waves in the water layer can lead to a better understanding of the mechanisms behind the noise as well as certain aspects of real field data.

In this study a Matlab code has been developed of the normal mode solution in a model that consists of a water layer on top of a homogeneous elastic half space. We will compare real noise recordings acquired by CGG in the North Sea with the output from this modeling code in the far-field (so called Pekeris waveguide model as described in Zhang and Tindle (1993b). The thesis consists of six main parts (chapters) organized as follows:

- This thesis begins with an introduction which discusses the basic characteristics of the underwater acoustic environment. The variation of sound speed in water with respect to temperature, salinity, depth, and hydrostatic pressure is illustrated and discussed.
- The second part focusses on the properties sound propagation in water, acoustic noise, and how transmission loss and attenuation depend on parameters like frequency and depth.
- The third chapter presents the theory behind normal mode solution for shallow water and includes the extension of Pekeris' theory to handle the case of normal mode sound propagation from an impulsive point source in a liquid layer overlying a semi-infinite elastic solid.

- In the fourth part we deal with the practical mode solution for shallow water and a more robust technique to solve for the wavenumbers is introduced.
- Chapter five gives results from the numerical simulations and comparisons with real data.
- Finally, chapter six gives main conclusion and recommendations for future work.

1.2 Under water acoustic environment

As indicated by Sablon et al. (2012) acoustic waves originate from a mechanical perturbation (longitudinal wave) and this perturbation will propagate away in the elastic medium by a propagation rate called sound speed or velocity (c). Hence the sound speed in water does not depend on the direction of the ray, therefore the names “sound speed” and “sound velocity” are often used interchangeably (Ross, 1987). Underwater acoustics is the study of the propagation of sound in water and the interaction of the mechanical waves that constitute sound with the water and its boundaries. Despite the complexity of the environment, sound is widely used in underwater applications just because it is indispensably transparent to acoustic waves (Buckingham, 1992)

However sound propagation in shallow water is a complex problem with a great number of applications in oceanography, geophysics, and seismology. As Brechovskich and Godin (1999) pointed out, the studies of acoustics in shallow water ocean environment have been attracting the interest of researchers up to the present day. This model features a very specific ocean environment restricted by the water surface at the top and by the seabed at the bottom. The important feature of this configuration is to enable the trapping of sound energy between these two interfaces which also favours the propagation of sound over long distances (Costa et al., 2013).

It is difficult to determine a strict criteria or the boundary of depths distinguishing the regions of “shallow water" from “deep water” with accuracy. The values of the characteristic parameters of the waveguide associated with “shallow water” may vary within broad ranges. They depend not only on the geometric dimensions of the wave guide but also on the frequency of the sound source and the interactions of sound with the background (Yang, 2007).

As Kacnel'son and Petnikov (2002) described, with reference to Brechovskich and Lysanov (1991) and Rytov et al. (1988), for a wave guide with a constant sound speed and an absolutely rigid bottom the maximum number of energy-carrying modes (normal waves) is determined by the simple relation $M = \frac{2H}{\lambda}$, where H is the depth of the waveguide and λ is the sound wave length. On the other hand analogues estimate for the maximum number of energy-carrying rays can be written in the form $\mathrm{M}' \approx \frac{2\mathrm{r}}{H}$, where the distance between the sound source and the receiver is r. Here energy-carrying rays, means rays passing along a waveguide path less than $\sqrt{2}r$. Comparison of these two estimates suggests that a region can be classified as shallow water if the following condition is satisfied:

$$r^2 \gg \frac{2H^2}{\lambda} \qquad (1.1)$$

Such condition implies that the number of rays exceeds the number of modes and that each mode-energy significantly exceeds the energy of each beam. This condition occurs in shallow water regions of the ocean to sound signals with frequencies lower than 500Hz.

Moreover in shallow water, with boundaries framed by the surface and bottom, the typical depth-to-wavelength ratio is about 10–100 (Wan, 2010) or it is quite flat over several tens of kilometers with water depth less than 200m (Yang, 2007). Shallow water environments are found on the continental shelf, a region which is important to human activities such as shipping, fishing, oil production, underwater communication etc. (Buckingham, 1992, Yang, 2007). Hence, shallow water acoustics is one of the most challenging areas of underwater acoustics, complex waveguide environment, and unpredictable sound wave propagation.

In general, as Wan (2010) explained, shallow water acoustics deals with strong sea bottom and surface interactions, multipath propagation, and often involves complex variability in the water column. In shallow water the sea bottom is the dominant factor in controlling the environmental influence which plays a vital role in underwater sound propagation (KUMAR, 1999).

Although the ocean is an extremely complicated acoustic medium, variations in speed of sound (c) in the ocean are relatively small or as a rule, variations of the sound velocity (c) lies between about 1450 m/s and 1540 m/s (Jensen et al., 1994).

Sound propagation in sea water is mathematically described by the wave equation, whose parameters and boundary conditions are descriptive of the sea environment. Normal mode

representation is one essential model to describe sound propagation in the sea. In this type of model the ocean environment is considered as horizontally stratified and with horizontal variation (Kragh et al., 2004). However the vertical variation in the layering is typically much larger than the horizontal variation, a fact that minimizes out-of-plane refraction, diffraction, and scattering with some notable exceptions (Kacnel'son and Petnikov, 2002). Moreover as illustrated in Figs 1.1, 1.2 and 1.3 the sound speed (c) in the sea is an increasing function of temperature (T), salinity (S), and hydrostatic pressure (P), wherein pressure is a function of depth (z). Calculation of the speed of sound, can be carried out according to Wilson's empirical formula (KUMAR, 1999) :

$$c(S,T,P) = c_0 + \Delta c_T + \Delta c_S + \Delta c_P + \Delta c_{STP} \qquad (1.2)$$

The value of each term and a more detailed description is given in *Appendix D*. In eq. (1.2) $c\ (S,T,P)$ is speed of sound (m/s), T is temperature (°C), S is salinity (grams of salt per liter of water (g/Kg)), and P is hydrostatic pressure (MPa).

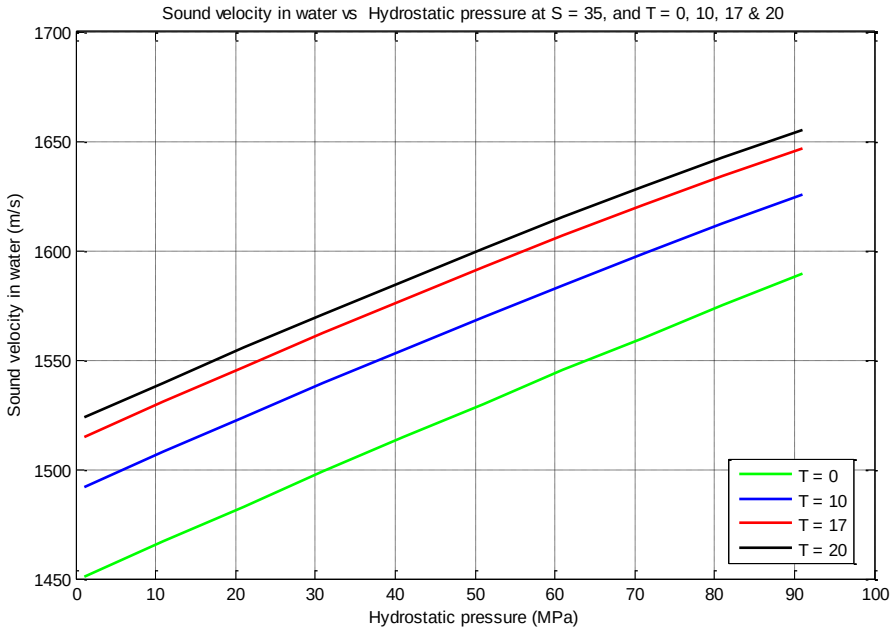

Figure: 1. 1 Variation of the velocity of sound in sea water with hydrostatic pressure at four different values of temperature T [℃]. *Salinity = 35g/Kg.*

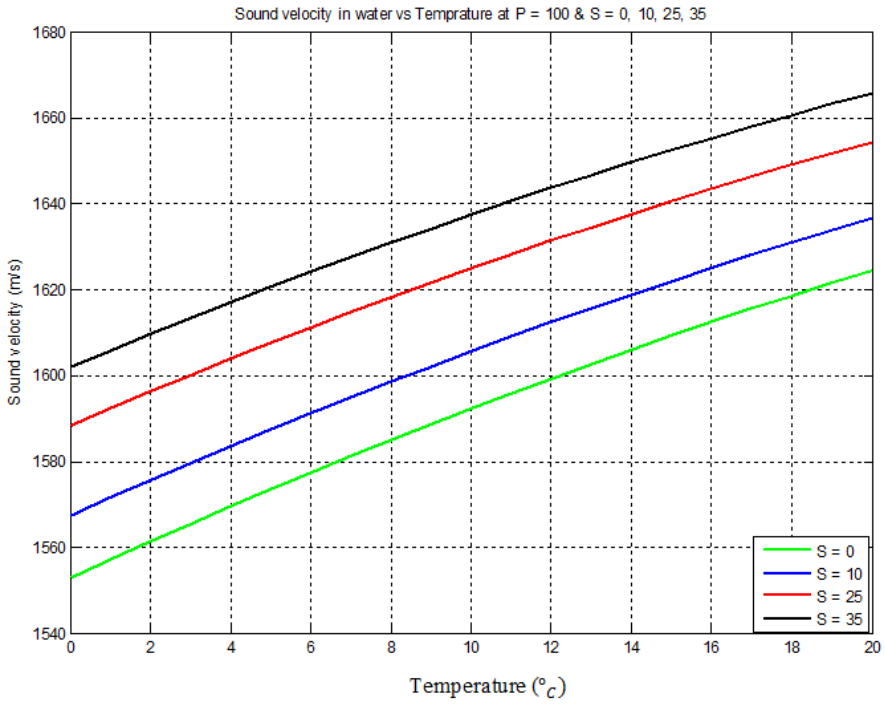

Figure: 1. 2 Variation of the velocity of sound in sea water with temperature T [℃]. *at different values of salinity S [g/Kg].*

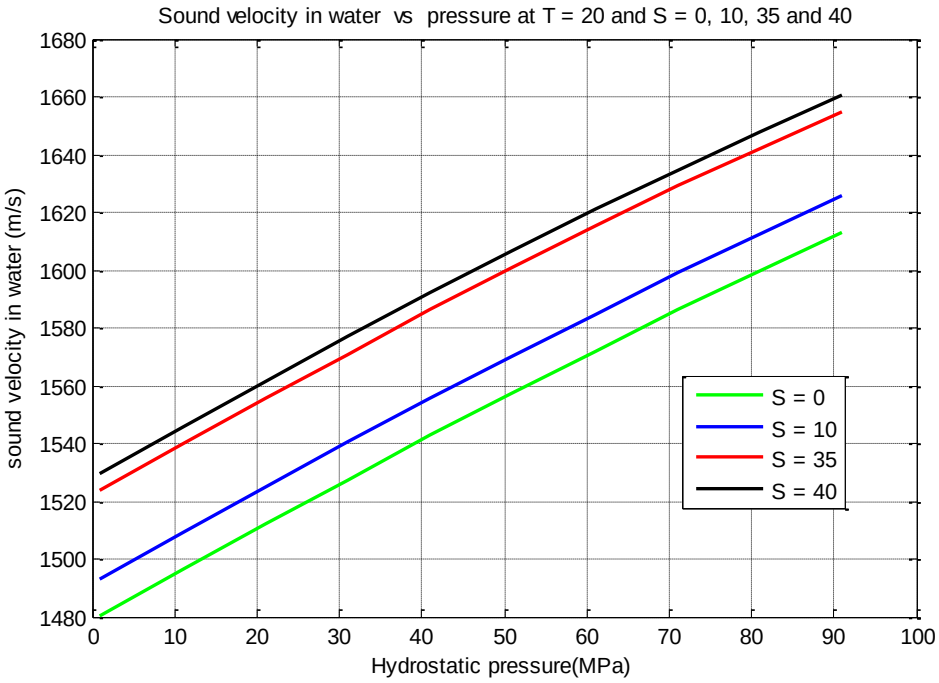

Figure: 1. 3 Variation of the velocity of sound in sea water with hydrostatic pressure at four different values of salinity S [g/Kg]. Temperature T = 20°C.

From the literature (Jensen et al., 1994, KUMAR, 1999) other empirical formulae exist like the one of Del Gresso valid for $0 < T[℃] < 32$, 22 < salinity [ppt] <45 and depths less than 1000 m:

$$c = 1449.2 + 4.6T - 0.055T^2 + 0.00029T^3 + (1.34 - 0.01T)(S - 35) + 0.016z \quad (1.3)$$

Meckenzie (1981) introduced an alternative formula which claims less standard error and without restriction of depth (Auld, 1973) :

$$\left.\begin{aligned} c = {} & 1448.96 + 4.591T - 0.05304T^2 + 0.0002374T^3 + 1.34(S - 35) + \\ & 0.0163z + 1.675 \times 10^{-7}z^2 - 1.025 \times 10^{-2}T(S - 35) - 7.139 \times 10^{-13}Tz^3 \end{aligned}\right\} \quad (1.4)$$

Figs. 1.4 and 1.5 show examples of use of Del Gresso empirical expression. Fig. 1.6 shows an example of use of Mackenzie's empirical formula. For most cases all these equation (within their limitations) are sufficiently accurate, though seasonal and diurnal changes affect the oceanographic parameters in the upper ocean and all of these parameters are a function of geography (Jensen et al., 1994).

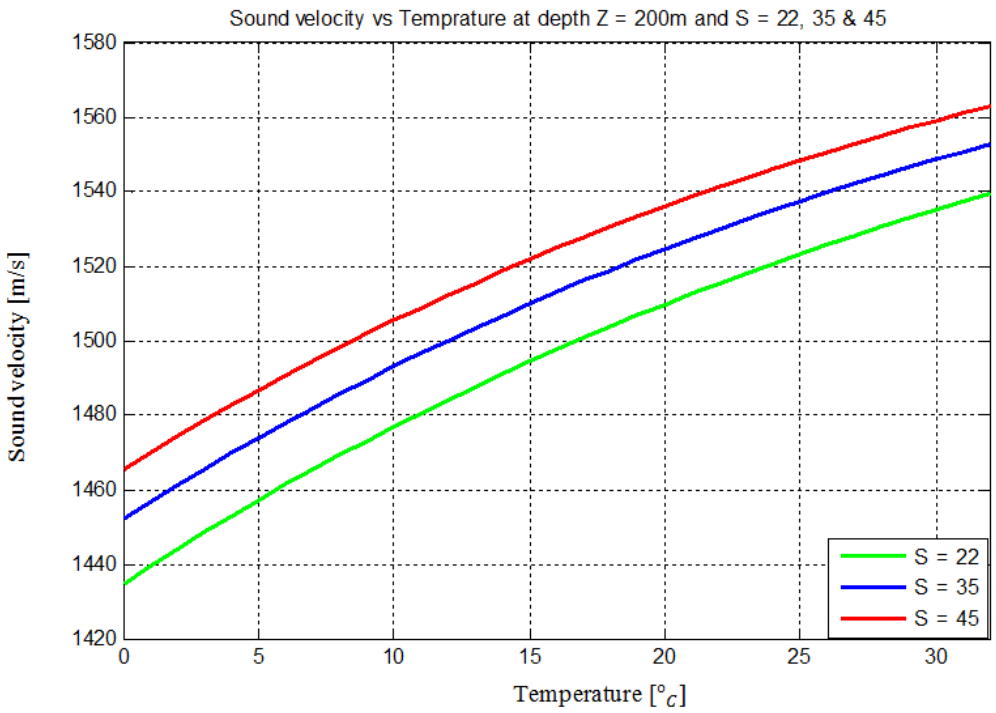

Figure: 1. 4 Variation of the velocity of sound in sea water with temperature at three different values of salinity (S = 22, 35, 45 g/Kg) and at a depth of 200 m (based on Del Grosso empirical formula).

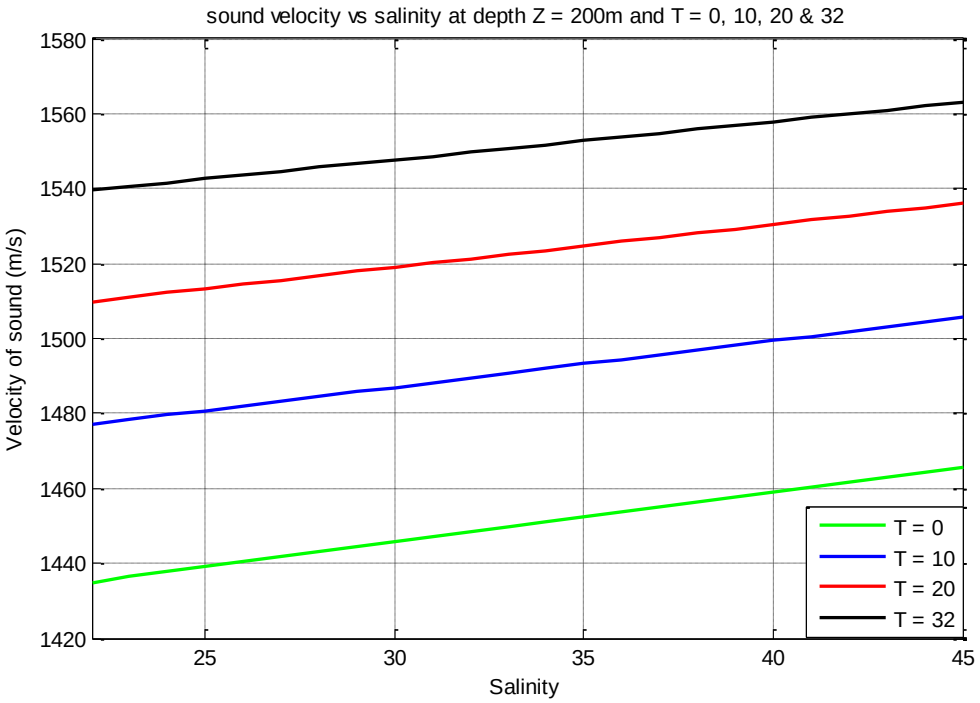

Figure: 1. 5 Variation of the velocity of sound in sea water with salinity at four values of temperature based on Del Grossos' empirical formula. (Depth of 200 m).

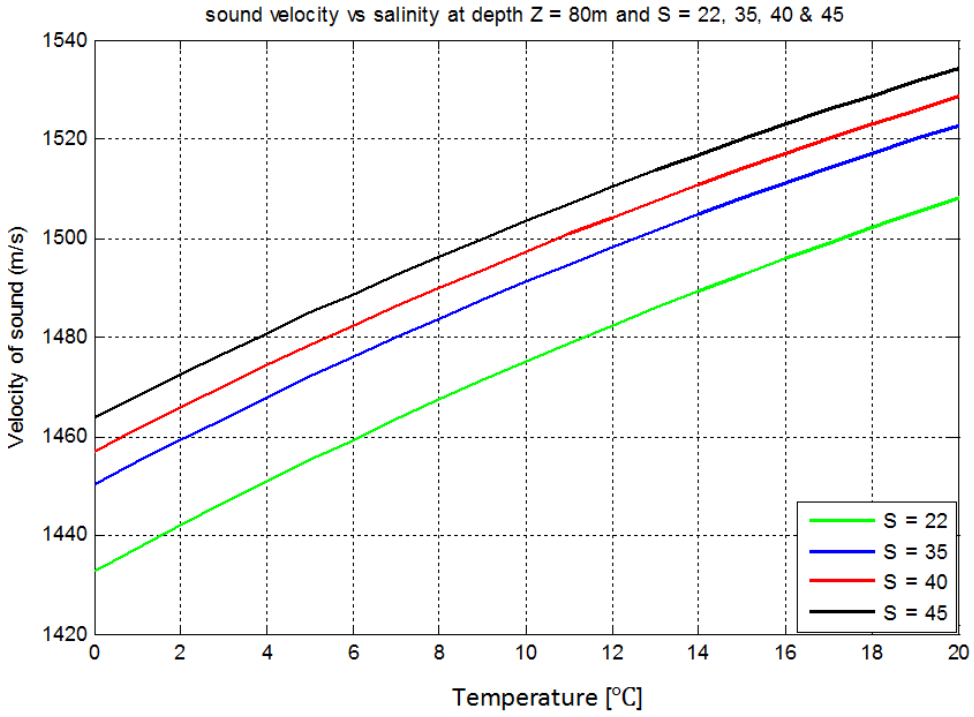

Figure: 1. 6 - Variation of the velocity of sound in sea water with temperature at five values of salinity [g/Kg] based on Mackenzie's empirical formula.

2. Propagation effects and acoustic noise

2.1 Attenuation and spreading loss

Acoustic waves are commonly used in underwater detection and communications. According to Sablon et al. (2012), the main factors that affect underwater acoustic propagation in the ocean/sea are loss and attenuation, refraction, scattering and noise. The accumulated decrease in acoustic intensity as an acoustic pressure wave propagates outwards from a source is known as a Transmission Loss (TL). As the acoustic wave propagates outwards from the source the intensity of the signal is reduced with increasing range due to either spreading or attenuation. So the various sources of loss of a sound wave may be categorized into spreading loss and attenuation loss (Urick, 1979).

Spreading loss is a measure of signal weakening due to the geometrical spreading of a wave propagating outward from the source. As the acoustic waves propagate outwards from the source the most visible process is their loss of the intensity of the signal with increasing range due to spreading (divergence effect). In the case of a point source of radiation, or at large distances from any source, the total transmitted power is spread over the surface of a sphere ($A = \pi r^2$) of radius r at range R. With the radius r increasing in proportion with the range R, the intensity is given by

$$I = \frac{P}{\pi r^2} \sim \frac{1}{R^2} \qquad (2.1)$$

Equation (2.1) depicts the inverse square law which tells us that the acoustic intensity is reduced in proportion to the square of the range due to spreading alone. Acoustic values are usually quantified on logarithmic scale and almost invariably expressed in [dB]. Due to the large range of sound intensities (from about for a barely whisper 10^{-9} W/m^2 to over a kW/m^2) and an approximately logarithmic acoustic stimuli of human response, logarithmic measurement units in acoustic were needed (Costa et al., 2013). Hence from the formal definition of spreading on the decibel scale:

$$TL_{sl} = 10 \log \left(\frac{Intensity\ at\ a\ distance\ of\ 1m}{Intensity\ at\ a\ distance\ R} \right)$$

$$TL_{sl} = 10\ log \left(\frac{P/2\pi(1m)^2}{P/2\pi R^2} \right)$$

$$TL_{sl} = 10\,log(R^2) = 20\,log(R) \qquad (2.2)$$

Since sea water is a dissipative propagation medium because of viscosity or chemical reactions, it absorbs a part of the transmitted wave energy. This leads to a proportional decrease of local amplitude with respect to the amplitude itself; hence the acoustic pressure decreases exponentially with distance and this will also contribute to spreading losses. Based on equation (2.2) (Spherical spreading law), Fig. 2.1 shows how TL varies with R in case of spreading losses only.

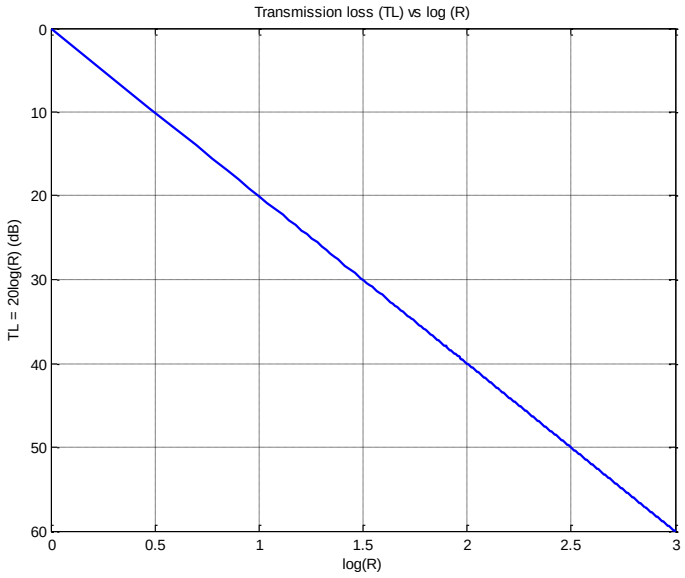

Figure: 2. 1 Transmission Loss (TL) as a function of range(R) with TL taking into account spreading losses only.

Scattering is reflection of sound in directions other than its original direction of propagation. Conversely absorption is the conversion of sound energy to other forms of energy. According to Soubaras et al. (2012a) wave attenuation is the loss in energy of a propagating wave due to the combined effects of absorption, spherical spreading and scattering by particles in the water column and is one of the main limiting factors on the usable range of frequencies.

Absorption is often the most limiting factor in acoustic propagation. As indicated by Filippi (1999) the absorption of sound in sea water depends on many factors; the most important being the temperature, the salinity and frequency among others. As described by Sablon et al. (2012) with reference to Auld (1973) the amount of absorption depends strongly on the propagation medium and frequency. The absorption increases very rapidly with frequency and

this means that transmission over long ranges requires relative low frequency, thus absorption of low frequency sound is weak and it will penetrate into the seafloor.

In sea water (which is made of a mix of pure water and dissolved salts), absorption comes from pure water viscosity and molecular relaxations (like magnesium sulfate (MgSO4) molecules below 100 kHz and Boric acid ($B(OH)_3$) molecules below 1kHz). In general Transmission loss (TL) due to attenuation is represented in the sonar equations in terms of an attenuation coefficient 'α' with the units of dB/m. Molecular relaxation comprises in the dissociation of some ionic compounds in solution due to local pressure variations caused by the acoustic wave. This process is dominant for sound absorption in sea water.

According to Ross (1987), for a moving water particle in a certain direction (+x), the net pressure in the +x-direction acting on the fluid particle is derived from the simple velocity-pressure relation for plane-wave solutions which follows the impedance relation *(See Appendix A):*

$$\frac{p}{u} = \pm(\rho c) \qquad (2.3)$$

where u is the particle velocity and $\pm$ sign is for a wave traveling either in the positive $(+)$ or negative $(-)$ x- direction and the term ρc is called the specific acoustic resistance (acoustic impedance). Acoustic impedance characterizes the relationship between the acting sound pressure and the resulting particle velocity and its value in sea water is about $1.5\text{x}10^5$ g/cm^{2}s and for air 42 g/cm^{2}s.

The energy involved in propagating acoustic waves through a fluid are due to the kinetic energy (particle motion) and potential energy (stress in elastic medium). Then for a plane wave, the acoustic intensity (I) of a sound wave is the average rate of flow of energy (or power) passing through a unit area (usually the area is 1m^2) normal to the direction of the wave propagation. Since the intensity I is a vector which possesses magnitude and direction normal to the unit area, then a plane wave traveling in $+x$- direction and unit area in yz-plane has an instantaneous intensity (I) expressed by the product of the instantaneous acoustic pressure (p) and the in-phase particle velocity along x-direction, u_x. Thus $I = pu_x$ and applying equation (2.3) we get

$$I = \frac{p^2}{\rho c} \qquad (2.4)$$

For an absorptive medium as explained by Urick (1979) a certain fraction of the intensity of the sound wave is lost (or converted to heat) for a given distance. If this fraction is $\frac{dI}{I}$ for range R we can write the absorption of a plane wave as:

$$\frac{dI}{I} = -ndR \qquad (2.5)$$

Where n is a proportionality coefficient and the minus sign denotes a loss of intensity.

In travelling from R_0 to R, the intensity I of the plane wave at R is related to its intensity I_0 at R_0 and then integrating both sides of equation (2.5) give:

$$\int_{I_0}^{I} \frac{dI}{I} = -\int_{R_0}^{R} ndx\,, \qquad implies \qquad \frac{I}{I_0} = e^{-n(R-R_0)}$$

Introducing $10n(log_{10}e) = \alpha$ as absorption coefficient gives,

$$10\,log\left(\frac{I}{I_0}\right) = -\alpha(R - R_0) \qquad (2.6)$$

In underwater sound it is common to express transmission ratio as transmission loss, since pressures and intensities usually decrease with increasing distance from the source. As mentioned by Costa et al. (2013), assuming the reference position to be closer to the source, then the transmission loss (TL) in dB in case of absorption is:

$$TL_{ab} = 10\,log\left(\frac{I}{I_0}\right) \qquad (2.7)$$

which in combination with equation (2.4) gives

$$TL_{ab} = 20\,log\left(\frac{P}{P_0}\right) \qquad (2.8)$$

where $I_0\ or\ P_0$ are reference values.

Following Ross (1987), the total transmission loss (TL) between the source and the field position is expressed as:

$$TL = TL_{sl} + TL_{ab} = 20\,log\left(\frac{R}{R_0}\right) + \alpha(R - R_0) \qquad (2.9)$$

In general as Jensen et al. (1994) described, when sound propagates in the ocean, part of the acoustic energy is continuously absorbed, i.e., the energy is transformed into heat. Moreover, sound is scattered by different kinds of inhomogeneity, also resulting in a decay of sound

intensity with range. Often it is not possible in real ocean experiments to distinguish between absorption and scattering effects; they both contribute to sound attenuation in seawater. Ever since the beginnings of underwater acoustics, a high amount of attention has been brought to modeling of absorption coefficients, and various models have been proposed.

Ross (1987) proposed, based on research results of François and Garrison (1982), an empirical formula for the attenuation in sea water based on the sum of two relaxation terms and a viscosity component (Clay and Medwin, 1977a):

$$\alpha = \frac{A_1 P_1 f_1 f^2}{f^2 + f_1^2} + \frac{A_2 P_2 f_2 f^2}{f^2 + f_2^2} + A_3 P_3 f^2 \qquad (2.10)$$

with α being the absorption coefficient in dB/km. The various coefficients in eq. (2.10) are expressed in terms of z = depth (m); T = Temperature (℃); S = salinity (parts/1000); and the relaxation frequencies f_1 for Boric acid and f_2 for Magnesium sulfate. Explicit values for these constants are given in *Appendix B*. A simplified expression for the frequency dependence ($f\ in\ kHz$) of the attenuation (α) in sea water was introduced by Jensen et al. (1994):

$$\alpha \approx 3.3 \times 10^{-3} + \frac{0.11 f^2}{4100 + f^2} + 3 \times 10^{-4} f^2 \qquad (2.11)$$

Even though the attenuation of sound in seawater has some dependence on temperature, pressure, salinity, and acidity (pH value), equation (2.11) is considered sufficiently accurate for most problems in ocean acoustics. Based on eqs (2.9) and (2.11) we can observe in Figs. 2.2 (a, b and c) below how α and TL depend on frequency as well as how TL varies with range for different frequencies.

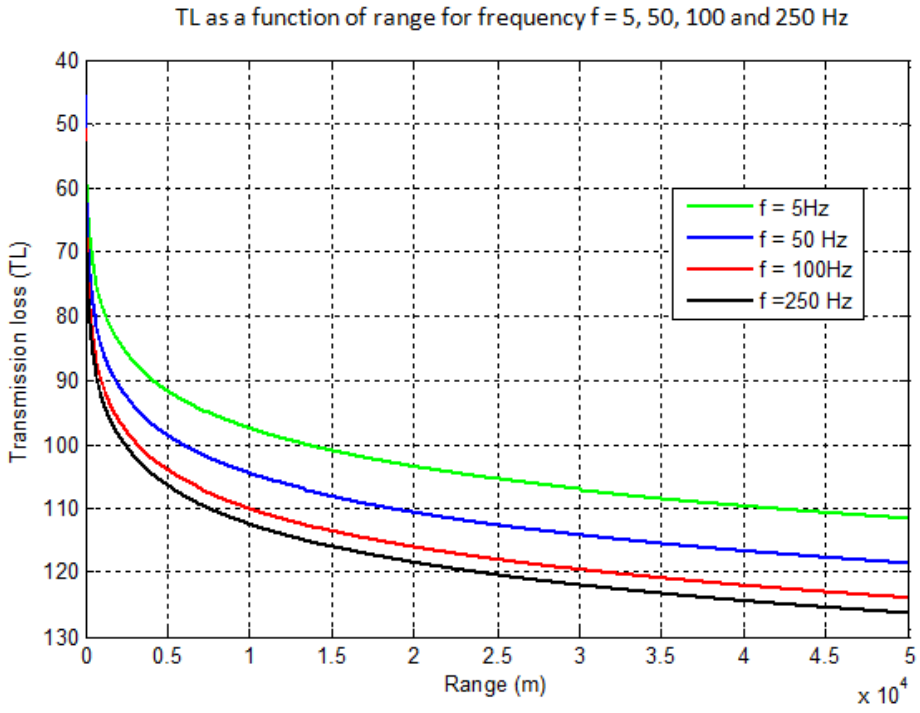
TL as a function of range for frequency f = 5, 50, 100 and 250 Hz
Transmission loss (TL)
Range (m)
x 10^4
f = 5Hz
f = 50 Hz
f = 100Hz
f =250 Hz

(a)

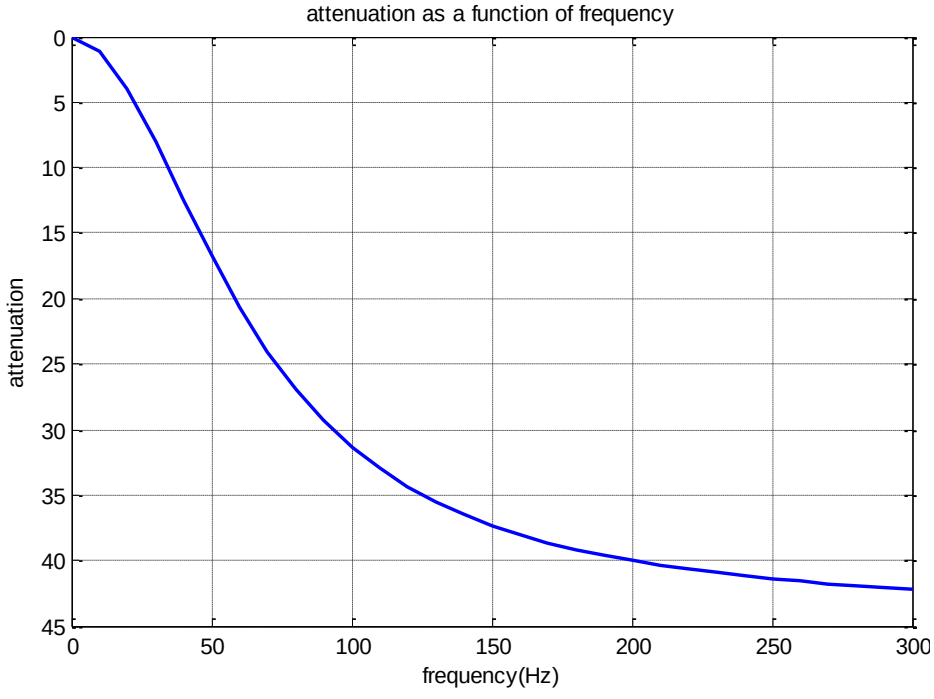
attenuation as a function of frequency
attenuation
frequency(Hz)

(b)

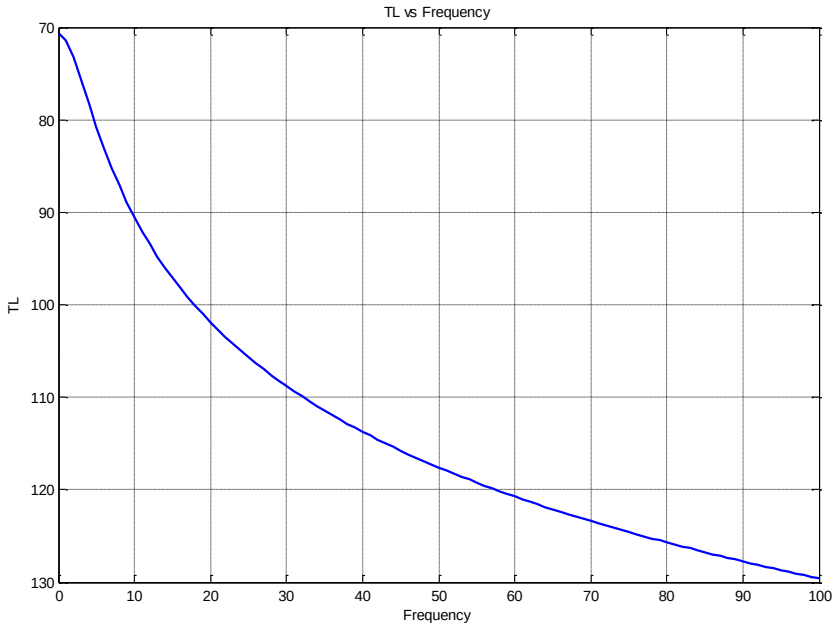

(c)

Figure: 2. 2 (a) TL as a function of range(R) for different frequency values with TL being plotted on a logarithmic scale. (b)Attenuation coefficient as a function of frequency (c)Transmission loss as a function of frequency.

Also depth is a very important factor for the absorption coefficient. If the frequency is high enough the relaxation effect of (MgSO4) is predominant, and it is often accurate enough to multiply the absorption coefficient at surface by the coefficient P_2 of Francois and Garrison's model *(see Appendix B).* Thus for the particular application concerned with the total absorption over the entire water column (for an echo sounder signal propagating from the source to the bottom and back to the source again), the integrated absorption will be:

$$\alpha(H) = \frac{1}{H}\int_0^H \alpha(z)dz \qquad (2.12)$$

Then neglecting the salinity and temperature variations with depth the mean coefficient of the total absorption (α) with respect to depth (H) is given as:

$$\alpha(H) = \alpha(0)\left[1 - 1.37 \times 10^{-4}\left(\frac{H}{2}\right) + 6.21 \times 10^{-9}\left(\frac{H^2}{3}\right)\right] \qquad (2.13)$$

or

$$\alpha(H) = \alpha(0)A(H) \qquad (2.14)$$

where $\alpha(0)$ is the absorption value at the surface and $A(H)$ is the absorption correlation term. A plot of the relation given in eq. (2.13) is shown in Fig. 2.3.

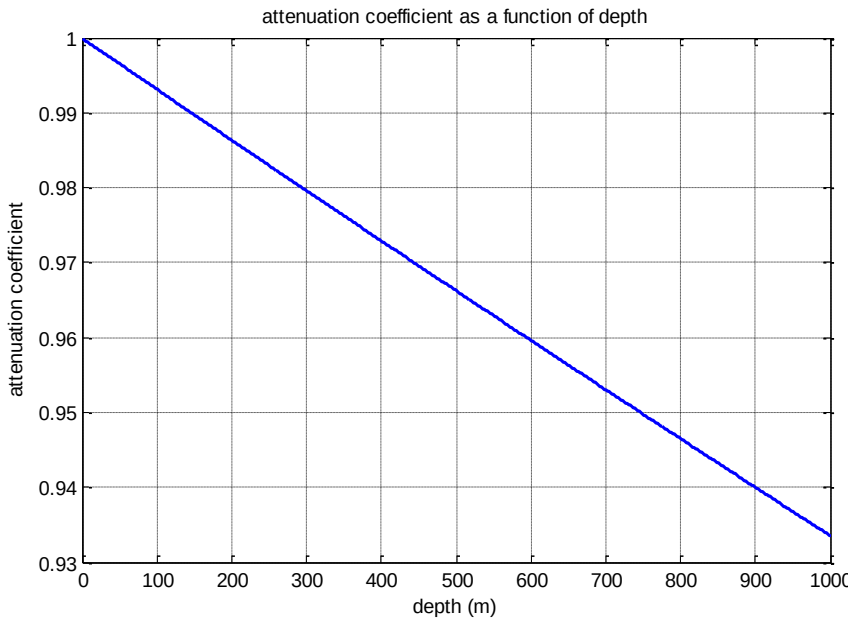

Figure: 2. 3 Attenuation coefficient as a function of depth

As clearly demonstrated in Figure (2.3), absorption is higher at shallow depth. But this result only shows more qualitatively the effect of depth on attenuation, without considering the exact temperature and salinity.

In general during its propagation, sound waves can be reflected, refracted, or attenuated by the medium. Therefore when sound travels through a medium, its intensity diminishes with distance. In idealized materials, sound pressure (signal amplitude) is only reduced by the spreading of the wave. Natural materials, however, all produce an effect which further weakens the sound because of the existence of both scattering and absorption. The combined effect of scattering and absorption is called attenuation.

As described by ORJI (2012), sea water contains considerable heterogeneity: like living organisms, bubble layers close to the surface, etc. This property of heterogeneity could represent potential scatterers of acoustic waves. Therefore the rough sea surface created by the turbulent ambient conditions (like winds above it) causes perturbations in the seismic data since the reflection response of the non-flat sea perturbs the seismic wavelet (Laws and Kragh, 2006).

The region in which turbulence exists is a function of depth and sea surface conditions. Clay and Medwin (1977a) discussed underwater motion and the depth dependence of the displacement amplitude. Thus, though material variation usually has a smaller acoustic effect than temperature variations, the motion of the medium is significant under certain

circumstances and may even overcome the temperature influence. For a simple long-crested wave in deep water, the vertical and horizontal components of the material velocity and the displacement are almost orbital near the surface. Hence the depth dependence of the displacement amplitude $''a''$ can be represented by

$$a = a_0 \, e^{-\frac{2\pi z}{\lambda}} \qquad (2.15)$$

where λ = surface wave length, z = depth and a_0 = orbital displacement amplitude (or un-attenuated amplitude of the propagating wave) at the surface. The amplitude a is the reduced amplitude after the wave has travelled a *depth* (z) from that initial location. Figure 2.4 shows amplitude a as a function of $depth$ (z)

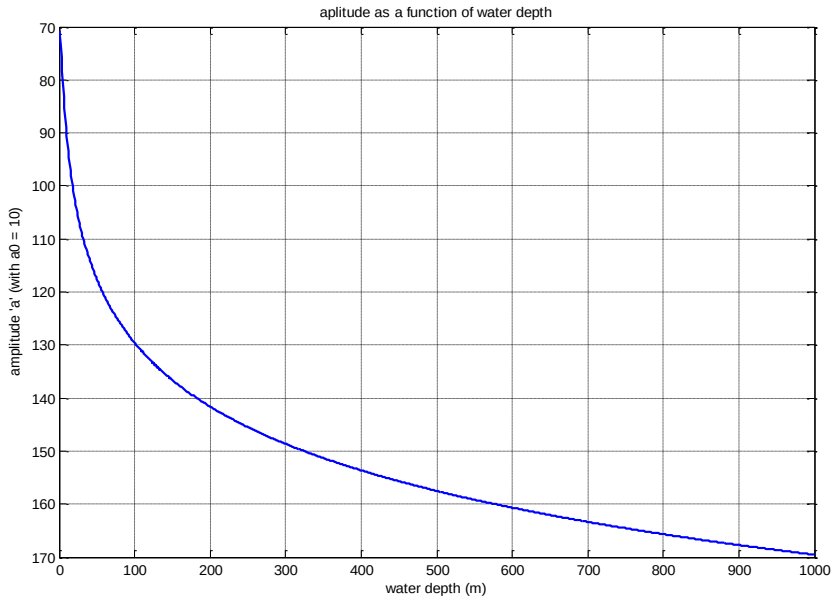

Figure: 2. 4 Amplitude a as a function of $depth$ (z)

The material displacement and particle velocity decrease exponentially with the increasing distance from the surface. Furthermore, Dunn's (1965) study cited in Clay and Medwin (1977b) shows that horizontally isotropic turbulence exist for large depth, and with an increasing degree of turbulence close to the surface. Consequently as stated by Hill et al. (2007), towing shallow sources and cables makes the data more susceptible to environmental noise, wherein the low frequencies needed for deep structural imaging and seismic inversion will be attenuated while deeply towed sources and deeply towed cable pairs (over/under acquisition) enhance the low frequencies, attenuate the high frequencies and the recorded data have a higher signal-to-ambient-noise ratio.

In conclusion, when acoustic waves propagate, the most visible process is their loss of intensity, because of geometrical spreading (divergency effect) and absorption of acoustic energy by the propagation medium itself. This propagation loss (or transmission loss) is a key parameter for acoustic systems, as it constrains the amplitude of the signal received, hence the receivers performance, directly dependent on the signal-to-noise ratio (Lurton, 2010).

2.2 Acoustic noise

Acoustic noise is an unavoidable basic limitation on the use of sound in the ocean/sea. There are a number of mechanisms responsible for generation of oceanic acoustic noise with different frequency ranges. Mainly categorized in to two types of noises: manmade and natural. The noise that originates from natural like ocean waves, rain, earthquakes, underwater volcanic eruptions, storms from distant, turbulence in the ocean and atmosphere, as well as some processes at the ocean surface can be considered as the natural background noise called ambient noise. Ambient noise is the usual unwanted background of sound which contains a great bulk of information concerning the state of the ocean surface, the atmosphere over the ocean, tectonic processes in the earth's crust under the ocean, the behaviour of marine animals and so on (Brechovskich and Lysanov , 2003).

In general, the challenge of sound propagation comes from the complexity of the environment. Background noise is also produced in water from different sources like electronic and mechanical operation of water vehicles and other human activities (manmade noise). In the frequency band 50–300 Hz underwater noise is mainly due to remote ship traffic. On the other hand, in the frequency band 0.5–50 kHz underwater noise is directly associated with the state of the ocean surface and the wind in the area considered. At frequencies above 100 kHz molecular thermal noise is dominant. Biological noise also produced by marine animals is relatively intensive only in some regions of the ocean and at certain periods of time (Brechovskich and Lysanov, 2003).

Given these potential sources of noise, echo sounder noise levels can change rapidly, perhaps through changes in environmental conditions, vessel speed or course, as well as bottom hardness or water depth which can affect the propagation of noise to the transducer (KUMAR, 1999)

3. Normal mode solution for shallow water

Sound propagation in the ocean is mathematically described by the wave equation, whose parameters and boundary conditions are descriptive of the ocean environment. Normal mode representation is among other types of models used to describe sound propagation in the sea/ocean. In this model it is considered that the ocean environment varies with depth and horizontal range (Kragh et al., 2004) . The normal mode theory of sound propagation in two and three liquid layers was given by Pekeris (1948) who solved the problem for waves originating from an impulsive point source located in the first layer of shallow water. As discussed by Urick (1979) this solution fully explains most of the characteristics of explosive sounds in shallow water. Pekeris theory can also be extended to handle the case of normal mode sound propagation from an impulsive point source in a liquid layer overlying a semi-infinite elastic solid (Press and Ewing, 1950). This is the type of model employed here.

Consider now propagation of elastic waves through a Pekeris type of waveguide model. A simple two-layer fluid-solid model consists of a homogeneous fluid layer (of thickness *h*, density ρ_1, and compressional wave velocity (sound speed in water c_1) bounded above by a free surface (z = 0) and overlying a semi-infinite elastic solid (of density ρ_2, compressional wave speed c_2, and shear wave speed c_s) (Fig 3.1). The water surface and the bottom are assumed plane and parallel. Attenuation (α_1, α_2, α_s) can be included by allowing the sound speeds or wavenumbers to have a small imaginary component.

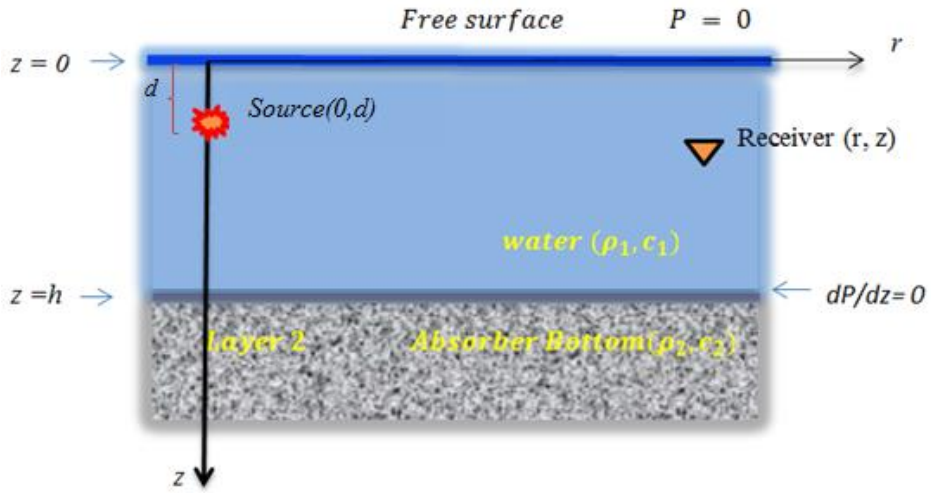

Figure: 3. 1 Two-layer waveguide model.

To solve for the normal modes, Ellis and Chapman (1985) introduced a cylindrical coordinate system in which the depth coordinate at the free surface ($z = 0$) increases with depth and where a point source of frequency $\omega = 2\pi f$ operates at depth z = d and range r = 0. The surface layer acts as a perfect reflector for waves with an angle of incidence greater than the critical angle from ray theory ($\theta > \theta_c$). In the Pekeris waveguide, the density of the fluid half-space (ρ_2) is greater than that of water (ρ_1), ($\rho_2 > \rho_1$), and the sound velocity in the underlying fluid half-space c_2 is greater than the compressional wave velocity in the water layer c_1, ($where\ c_2 > c_1$) (Ewing et al., 1957). The distortional wave velocity (or shear velocity) is represented by c_s.

The linear approximations which lead to the acoustic wave equation is typically written and solved in terms of pressure, displacement, or velocity potentials. These potentials are solutions of the wave equations (Ewing et al., 1957). Thus the potentials (ϕ_i) determined from the component displacements q_1 and w_1 and the pressure p_1 due to a point source of compressional waves at $r = 0, z = d$ can be obtained. The wave equation is most often solved in the frequency domain and to determine the normal mode solutions which predominate at large distances from the source, we follow the procedure of Lamb (1904) and omit the time factor of simple harmonic motion $e^{i\omega t}$ for simplicity.

According to Katsnelson and Petnikov (2002) the solution of a plane wave equation of motion can be separated into a longitudinal P-wave part (which is the gradient of the scalar potential $\phi(r,z)$) plus a transverse S-wave part (which is the curl of a vector potential $\psi(r,z)$)[1]. These two waves travel independently with different velocities. The Helmholtz decomposition of a vector field states that, in general any arbitrary vector field can be represented as a sum of curl-free and divergence-free forms. Then the Helmholtz decomposition of the elastic displacement field $\bar{q}$ is given by

$$\left.\begin{aligned} &\bar{q} = \nabla\phi + \nabla \times \psi_2\ ,\quad \nabla.\psi_2 = 0,\ \nabla \times \phi = 0 \\ &\bar{q} = \bar{q}_{P-wave} + \bar{q}_{S-wave} \\ &\Rightarrow\ \nabla \times \bar{q}_{P-wave} = \nabla \times (\nabla\phi) = 0 \\ &\Rightarrow \nabla.\bar{q}_{S-wave} = \nabla \times (\nabla \times \psi_2) = 0 \end{aligned}\right\} \qquad (3.1)$$

[1] The scalar potential $\phi(r,z)$ and the vector potential $\psi(r,z)$ are often called "Lame potentials" or P-wave and S- wave potentials, or "dilatational and rotational displacement potential," respectively.

We note that the vector potential has only two independent components. The part of ψ_2 that can be expressed as a gradient of scalar is discarded, whereas the part that has zero divergence is used. Thus:

$$\nabla.\bar{q}_{P-wave} = \nabla^2\phi;\ \nabla.\bar{q}_{S-wave} = 0$$

$$\nabla \times \bar{q}_{S-wave} = \nabla \times (\nabla \times \psi_2);\ \nabla.\bar{q}_{P-wave} = 0$$

If the radial and the vertical components of displacement are denoted by q and w respectively, they can be further expressed in terms of the compressional P-wave scalar potential $\phi(r,z)$ and the vertically polarized S-wave vector potential $\psi(r,z)$ as follows,

$$\left.\begin{aligned} q_1 &= \partial\phi_1/\partial r \\ w_1 &= \partial\phi_1/\partial z \\ q_2 &= \frac{\partial\phi_2}{\partial r} + \frac{\partial^2\psi_2}{\partial r\partial z} \\ w_2 &= \frac{\partial\phi_2}{\partial z} + \frac{\partial^2\psi_2}{\partial z^2} + \omega^2/{c_s}^2\psi_2 \end{aligned}\right\} \qquad (3.2)$$

Employing Hook's law the vertical stress p_{zz} and the tangential stress p_{zr} can be expressed in terms of q, w, ϕ, ψ and the elastic constants as follows:

$$p_{zz} = \lambda\nabla^2\phi + 2\mu\partial w/\partial z \qquad (3.3)$$

$$p_{zr} = \mu\left(\frac{\partial q}{\partial z} + \frac{\partial w}{\partial r}\right) \qquad (3.4)$$

Since the potentials are solutions of the wave equations and it is required that they satisfy the wave equations, thus for reduced simple harmonic motion:

$$(\nabla^2 + \omega^2/c_1^2)\phi_1 = 0,\ 0 \le z \le h \qquad (3.5)$$

$$(\nabla^2 + \omega^2/c_2^2)\phi_2 = 0\ ,\ z > h \qquad (3.6)$$

$$(\nabla^2 + \omega^2/{c_s}^2)\psi_2 = 0,\ z > h \qquad (3.7)$$

Where $k_w = \frac{\omega}{c_1}$, $k_2 = \frac{\omega}{c_2}$, $k_s = \frac{\omega}{c_s}$ and $\nabla^2 = \frac{\partial^2}{\partial r^2} + \frac{1}{r}\frac{\partial}{\partial r} + \frac{\partial^2}{\partial z^2}$

For a viscous fluid there is adhesion and the conditions are the same as for a bond between two solids. However for an interface between a perfect (i.e. non-viscous) fluid and a solid (fluid-solid interface) continuity holds (Filippi, 1999) and hence the normal stress p_{zz} at the surface of the sea must be continuous at all points on the boundary while the tangential stress

p_{rz} at the interface vanishes (free slip surface) and no contribution from the horizontal (tangential) displacement at the interface (Jensen et al., 1994, Auld, 1973). Therefore both the vertical stress and the vertical displacement have to be continuous at the interface. Thus the solutions of (3.3), (3.4), and (3.5) must satisfy the boundary conditions:

$$(p_{zz})_1 = 0 \;\; at\; z = 0 \tag{3.8}$$

$$(p_{zz})_{1'} = (p_{zz})_2 \;\; at\; z = h \tag{3.9}$$

$$(p_{zr})_2 \; = 0\; at\; z = h \tag{3.10}$$

$$w_{1'} \; = w_2 \quad at\; z = h \tag{3.11}$$

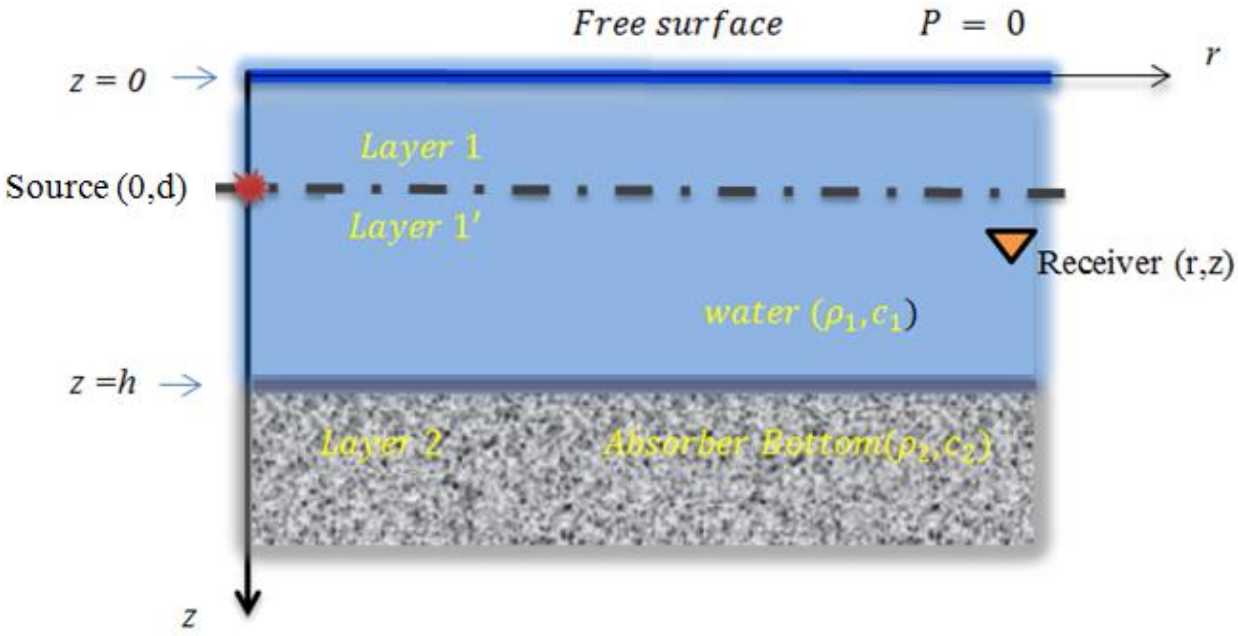

Figure: 3. 2 Solution domains for waveguide problem.

The primed symbols refers to the fact that the fluid above and below the source moves in opposite directions and we need to divide the water into two regions as shown in fig. 3.2. This implies the typical solutions for eqs. (3.3) – (3.5) are the form (Press and Ewing, 1950):

$$\phi_1 = A\, sin(\gamma z)\, J_0(kr) \quad 0 \le z \le d \tag{3.12}$$

$$\phi_{1'} = [B\, sin(\gamma z) + C cos(\gamma z)] J_0(kr) \quad d \le z \le h \tag{3.13}$$

$$\phi_2 = D e^{-\eta z} J_0(kr) \qquad z > h \tag{3.14}$$

$$\psi_2 = E e^{-\beta z} J_0(kr) \qquad z > h \tag{3.15}$$

Where the separation constants γ, η and β are obtained by substituting eqs. (3.12) – (3.15) in eqs. (3.3) – (3.5) and can be written as:

$$\left.\begin{aligned} \gamma &= \sqrt{(\omega/c_1)^2 - k^2} \\ \eta &= \sqrt{k^2 - (\omega/c_2)^2} \\ \beta &= \sqrt{k^2 - (\omega/c_s)^2} \end{aligned}\right\} \qquad (3.16)$$

γ, η, β are positive real or negative imaginary following the convention of Pekeris (1948). Note that ϕ_1 in eq. (3.12) has been chosen to satisfy the boundary condition in eq. (3.8).

From eqs. (3.12) – (3.15) it follows that we need to solve for five unknowns A, B, C, D and E. Thus we need the same number of boundary conditions (BC). The three first BC's are given by eqs. (3.9) – (3.11). The two last ones are additional BC's needed to match the two solutions ϕ_1 and $\phi_{1'}$ in the water layer. They read as follows:

$$(p_{zz})_1 = (p_{zz})_{1'} \quad at\ z = d \qquad (3.17)$$

$$\left(\frac{\partial \phi_1}{\partial z}\right) - \left(\frac{\partial \phi_1}{\partial z}\right)' = 2ZJ_0(kr) \qquad (3.18)$$

How to choose the quantity Z and also details about how to arrive on the final solutions the reader is referred to Urick (1979). Since our interests are in wave modes in the water layer, we only state the solutions obtained for ϕ_1 and $\phi_{1'}$:

$$\phi_1 = 2e^{i\omega t}\int_0^\infty J_0(kr)kdk\,\frac{sin(\gamma z)}{\gamma}\left\{\frac{\frac{\rho_1\omega^4\eta}{\rho_2{c_s}^4\gamma}sin\,\gamma(h-d) - \left[4k^2\eta\beta - \left(2k^2 - \frac{\omega^2}{{c_s}^2}\right)^2\right]cos(\gamma(h-d))}{\frac{\rho_1\omega^4\eta}{\rho_2{c_s}^4\gamma}sin(\gamma h) - \left[4k^2\eta\beta - \left(2k^2 - \frac{\omega^2}{{c_s}^2}\right)^2\right]cos(\gamma h)}\right\} \qquad (3.19)$$

$$\phi_{1'} = 2e^{i\omega t}\int_0^\infty J_0(kr)kdk\,\frac{sin(\gamma d)}{\gamma}\left\{\frac{\frac{\rho_1\omega^4\eta}{\rho_2{c_s}^4\gamma}sin\,\gamma(h-z) - \left[4k^2\eta\beta - \left(2k^2 - \frac{\omega^2}{{c_s}^2}\right)^2\right]cos(\gamma(h-z))}{\frac{\rho_1\omega^4\eta}{\rho_2{c_s}^4\gamma}sin(\gamma z) - \left[4k^2\eta\beta - \left(2k^2 - \frac{\omega^2}{{c_s}^2}\right)^2\right]cos(\gamma z)}\right\} \qquad (3.20)$$

The expressions in eqs. (3.19) and (3.20) can be further elaborated on by residue analysis. Thus these solutions can be expressed as the sum of the residues of the integrals and two integrals along branch lines corresponding to the branch points $k_2 = \omega/c_2$ and $k_s = \omega/c_s$. The residues which diminish as $r^{-1/2}$ gives the normal mode solutions, whereas the branch line integrals diminish as r^{-2}, and become negligible for large r. Thus we neglect these contributions here. From the residue analysis we arrive on the following solution ($\phi_1 = \phi_{1'}$ and also using the asymptotic version of the Hankel function) (Press and Ewing, 1950):

$$\phi_1 = \frac{2\pi}{h}\sqrt{\frac{2}{\pi r}}\sum_n \frac{1}{\sqrt{k_n}}\exp\left[i\left(\omega t - k_n r - \frac{\pi}{4}\right)\right] \quad k_n h \frac{sin(\gamma z)}{\gamma}\left\{\frac{\frac{\rho_1\omega^4\eta}{\rho_2 c_s{}^4\gamma}sin\,\gamma(h-z) - \left[4k^2\eta\beta - \left(2k^2 - \frac{\omega^2}{c_s{}^2}\right)^2\right]cos(\gamma(h-z))}{\frac{\partial}{\partial k}\left\{\frac{\rho_1\omega^4\eta}{\rho_2 c_s{}^4\gamma}sin(\gamma z) - \left[4k^2\eta\beta - \left(2k^2 - \frac{\omega^2}{c_s{}^2}\right)^2\right]cos(\gamma z)\right\}}\right\} \quad (3.21)$$

for $0 \leq z \leq d$

In general, marine data are often contaminated by guided waves that travel horizontally within the water layer or in the layer or layers beneath the water layer. Guided waves are dispersive, which means that each frequency component travels at a different speed; namely the horizontal phase velocity. The dispersive character of guided waves is most pronounced in shallow environments (basically less than 100 m of depth). Depending on various water-bottom conditions the character of these waves may vary from shot to shot or they can also cause linear noise on stacked data and are easily confused with the linear noise that is associated with side scatterers.

In eq. (3.21) k_n is the horizontal wavenumber of the n^{th} mode and the subscript n indicates that solutions which satisfy both the differential equation and the boundary conditions at the interfaces are obtained only for certain values (the eigenvalues) of the horizontal wavenumber k. The quantity is to be evaluated at $k = k_n$ where k_n are the roots of the period equation obtained by setting the denominators of eqs. (3.19) and (3.20) equal to zero, i.e.

$$\frac{\rho_1}{\rho_2}\frac{\omega^4}{c_s{}^4}\frac{\eta}{\gamma}sin(\gamma z) - \left[4k_n^2\eta\beta - \left(2k^2 - \frac{\omega^2}{c_s{}^2}\right)^2\right] = 0 \quad (3.22)$$

$$tan(\gamma h) = -\frac{\rho_2\gamma}{\rho_1\eta}\left[\left(1 - \frac{2k_n^2}{\left(\frac{\omega}{c_s}\right)^2}\right)^2 + \frac{4k_n^2\eta\beta}{\left(\frac{\omega}{c_s}\right)^4}\right] = -\frac{\rho_2\gamma_n}{\rho_1\eta_n}\,p(k_n) \quad (3.23)$$

$$\textit{where} \quad P(k_n) = \left(1 - \frac{2k^2}{(\omega/c_s)^2}\right)^2 + \frac{i4\eta\beta k^2}{(\omega/c_s)^4} \quad (3.24)$$

k_n is the horizontal wavenumber of a horizontal wave travelling down the wave guide with the phase velocity of $c_n = \frac{\omega}{c_n}$ and β is the vertical wave number for shear waves in the bottom. Eq(3.23) is the transcendental equation in k_n with real roots of range of discreet eigenvalues: $minimum\ (k_2) = \frac{\omega}{c_2} < k_n < maximum\ (k_1) = \frac{\omega}{c_1}$.

By introducing pressure, the final normal mode solution can be written on the form (Zhang and Tindle, 1993a)

$$p(r,z) = \left(\frac{2\pi}{r}\right)^{1/2} e^{\frac{i\pi}{4}}\sum_n N_n^2 sin(\gamma_n z)\,sin(\gamma_n d)\,(k_n{}^{-1/2})e^{ik_n r} \quad (3.25)$$

In eq. (3.25) the normalization factor N_n is given explicitly as

$$N_n = \left[\left(\frac{H}{2} + \frac{\sin(2\,k_{zn}h)}{4\,k_{zn}} + \frac{\rho_1 sin^2(\,k_{zn}h)}{2\rho_2\eta_n}\frac{A\,(k_n)}{p^2\,(k_n)}\right)\right]^{-1/2} \tag{3.26}$$

where

$$A\,(k_n) = \left(1 - \frac{2{k_n}^2}{(\omega/c_s)^2}\right)^2 + \frac{8\eta_n^2}{(\omega/c_s)^2}\left(1 - \frac{2{k_n}^2}{(\omega/c_s)^2}\right) - \frac{i4\eta_n^3}{\beta_n(\omega/c_s)^2}\left(2 - \frac{3{k_n}^2}{(\omega/c_s)^2}\right) \tag{3.27}$$

When there are no shear waves and no attenuation, this normal mode solution is a sum over a set of "trapped" modes and a sum over a set of "leaky" modes. The trapped modes are called so because they have real eigenvalues and correspond to rays which are totally internally reflected at the ocean bottom. The leaky modes have complex eigenvalues and loose energy to the ocean bottom and decay rapidly with range. On the other hand when there is attenuation (and/or a solid bottom with a low shear speed) all normal mode eigenvalues are complex and the simple distinction between trapped and leaky modes is lost. All eigenvalues are complex and all modes decay with range (Jensen et al., 1994). Thus based on the above relations both trapped and leaky normal modes can be treated and the attenuation of the leaky modes generally increases as mode number increase (Zhang and Tindle, 1993b).

4. Practical mode solution for shallow water

In order to solve eq. (3.25), we need to find all eigenvalues of k (k_n) from eq. (3.23). This equation is of a transcended character and difficult to solve numerically. In this chapter a more robust technique to solve for k_n is introduced.

Weston (1959) introduced the concept of the effective boundary depth and stated that one could view the reflection as taking place at an imaginary pressure release boundary located at a specific depth below the true boundary (Chapman and Ward, 1989). Thus the effective depth concept concerns the reflection process at sea bottom and the geometry of this concept is shown below (Figure: 4.1):

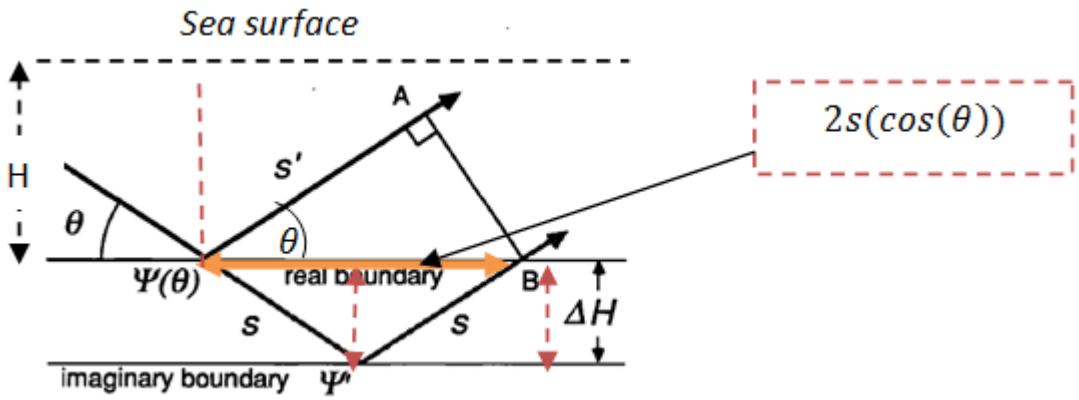

Figure: 4. 1 Geometry used to derive the effective boundary depth (adapted from Chapman and Ward (1989)).

The derivation of the geometry of the effective boundary depth by Chapman and Ward (1989) is based on the following assumption. A plane wave with frequency of f (corresponding angular frequency of $\omega = 2\pi f$) in a fluid medium of sound speed c_1 is incident upon a plane boundary with another acoustic medium, such that its wave normal forms a grazing angle θ with the boundary plane. The wave is reflected from the interface with phase change of $\psi(\theta)$. A ray with an infinite plane wave front AB can represent an identical reflection with a constant phase change ψ' at an imaginary boundary located at some assumed depth $\Delta H(\theta)$ below. From Fig. 4.1 we see that the ray segments s and s' are given by the trigonometric relations:

$$s = \frac{\Delta H}{sin\theta} \quad and \quad s' = 2scos^2\theta = \frac{2\Delta H cos^2\theta}{sin\theta} \qquad (4.1)$$

Relative the phase of the incident wave at the boundary, the phase of the reflected plane wave at points A and B is given by

$$\Phi_A = k_w s' + \psi(\theta) \quad and \; \Phi_B = 2k_w s + \psi' \qquad (4.2)$$

in which $k_w = k = \frac{\omega}{c_1}$. For A and B to lie on the same wave front then, $\Phi_A = \Phi_B$ and after proper substitution (see *Appendix C*) we get:

$$\Delta H(k) = \frac{\psi(k) - \psi'}{2k_w sin\theta} \qquad (4.3)$$

Equation (4.3) describes the concept of effective depth of a Pekeris channel with a fluid/elastic boundary incorporating shear-wave effects in the seabed (Zhang and Tindle, 1993b). $\psi(k)$ and $\psi'(k)$ are the phase change on reflection from respectively the real boundary and the pressure-release (imaginary) boundary; (where $\psi' = -\pi$) and θ is the grazing angle. Then the effective depth approximation is obtained by rewriting equation (4.3) as follows

$$\Delta H(k) = \frac{[\psi(k)+\pi]c_1}{2\omega sin\theta} = \frac{[\psi(k)+\pi]}{2\gamma(k)} \qquad (4.4)$$

The parameter k is the wave number for horizontal propagation and its values that satisfy Eq. (4.3) are identified as the eigenvalues k_n of the normal modes. The horizontal wave number (k) and the vertical wave number (γ) are related to the ray incident angle (θ) (plane wave fronts)

$$k_w = k = \left(\frac{\omega}{c_1}\right) cos\theta \qquad (4.5)$$

$$and$$

$$\gamma = \left(\frac{\omega}{c_1}\right) sin\theta = \sqrt{\left(\frac{\omega^2}{c_1^2} - k^2\right)} \qquad (4.6)$$

The real effective depth is calculated by taking the real part of the limit as $k \to \omega/c_1$.

For a moment we return to the physical shallow-water waveguide of depth H. Zhang and Tindle (1993b) demonstrated that the normal mode eigenvalues in a shallow water isovelocity waveguide of depth *H* are found by calculating the zeroes of a Wronskian, (thus k_n is the zeroes of Wronskian) and this leads to the following eigenvalue condition:

$$[1 + V(k_n) exp(i2\gamma H)]_{k=k_n} = 0 \qquad (4.7)$$

For a fluid over an elastic solid bottom the reflection coefficient $V(k_n)$ can be expressed as:

$$V(k_n) = \frac{\rho_2 \gamma P(k) - i\rho_1 \eta}{\rho_1 \gamma P(k) + i\rho_1 \eta} \qquad (4.8)$$

The parameters $\eta \; and \; \beta$ are the vertical wave number for compressional and shear waves in the bottom layer. In case of a shear wave speed $c_s = 0$, the parameter $P(k) = 1$ and the reflection coefficient reduces to that for a fluid-fluid interface:

$$V(k_n) = \frac{\rho_2 \gamma - i\rho_1 \eta}{\rho_2 \gamma + i\rho_1 \eta} \qquad (4.9)$$

The values of k which satisfy eq.(4.7) are identified as the eigenvalues k_n of the normal modes and hence $2\gamma H = \psi(k)$ is the complex phase shift of the reflection coefficient. From eq. (4.7) it also follows

$$\psi(k) = -ilnV(k_n) \qquad (4.10)$$

The real part of $\psi(k)$ represents the actual phase of the reflection coefficient while the imaginary part is directly related to the reflection losses. If the imaginary part of $\psi(k) = 0$ it represents the case of total reflection; and which means $|V| = 1$. This argument also leads to

$$\psi(k) + 2\gamma(k)H - \pi = 2(n-1)\pi \qquad (4.11)$$

where n is an integer and the eigenvalues k_n are the values of k satisfying equation (4.11). The first term ($n = 1$) represents the phase accumulated in the water by a plane wave with vertical wave number $\gamma(k)$, which travels up and down once in the wave guide, but for the second and third terms the phase changes from reflection at bottom and surface, respectively. Therefore equation (4.11) expresses the physical condition that, in order to persist in the waveguide, the total phase change of the wave in one complete cycle up and down must be a multiple of 2π. Waves with these particular wave numbers and corresponding angles reinforce and form the normal modes.

As explained by Zhang and Tindle (1993b), the approximate effective depth of the Pekeris channel is given by $H + \Delta H(k)$. Rewriting and equating eqs. (4.4) and (4.11) leads to:

$$\left.\begin{aligned} \psi(k) &= \Delta H(k) 2\gamma(k) - \pi, \;\; and \\ \psi(k) &= -2\gamma(k)H + \pi + 2(n-1)\pi \\ \psi(k) &= -2\gamma(k)H + \pi + 2n\pi - 2\pi, \quad implies \\ \Delta H(k)2\gamma(k) - \pi &= -2\gamma(k)H + \pi + 2n\pi - 2\pi \\ \Delta H(k)2\gamma(k) &= -2\gamma(k)H + 2n\pi \end{aligned}\right\} \qquad (4.12)$$

The eigenvalue equation for the vertical wave number of a normal mode in a perfectly reflecting isovelocity waveguide of depth $H + \Delta H(k) = H_{eff}$ can then be written as

$$\gamma_n = \frac{n\pi}{H+\Delta H(k)} = \frac{n\pi}{H_{eff}} \qquad (4.13)$$

Since long range propagation is dominated by rays of low grazing angle, we assume that the effective boundary shift ΔH(k) is almost constant and close to its value at $\theta = 0$ ($k = \omega/c_1$). The approximate eigenvalues can now be obtained by calculating γ_n (using equation 4.13) and finding the corresponding eigenvalues k_n using

$$k_n = \left(\frac{\omega^2}{c_1^2} - \gamma_n^2\right)^{1/2} \qquad (4.14)$$

These computations are done in an iterative manner as shown schematically in Fig. 4.2. This iterative loop for a fixed n starts by assigning k an intial value from the use of eq. (4.5) with a small grazing angle (f.ex.0.15°). Next, eq. (4.6) is used to calculate γ and eqs. (4.8) and (4.10) are employed to calculate ψ(k). We are now in the position to calculate ΔH from eq. (4.4) followed by calculating γ_n from eq. (4.13). Finally, an updated value of k_n can be found from eq.(4.14). This latter value is employed as a new initial value, and the iterative loop is repeated until a convergency criterion is fulfilled.

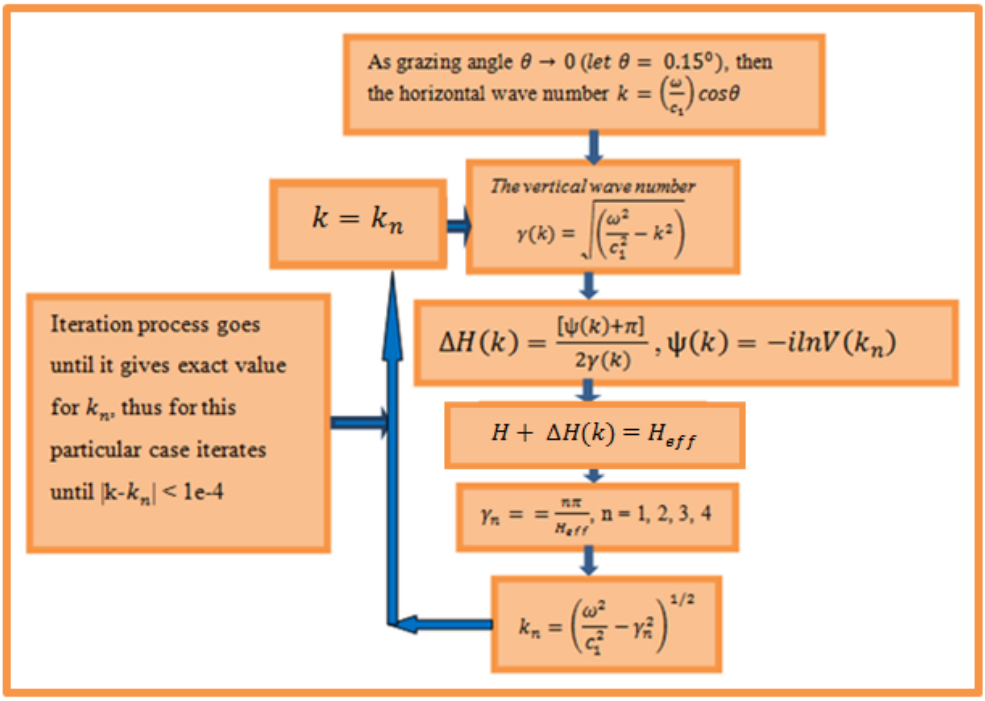

Figure: 4. 2 the schematic diagram for the iteration to obtain more accurate eigenvalues.

As already discussed, the real part of $\psi(k)$ represents the actual phase of the reflection and the complex (imaginary) part is related to the reflection losses. If the parameter $\psi(k)$ in the

above equations is complex, then the wavenumber k_n and the effective boundary shift $\Delta H(k)$ automatically become complex. Energy loss arises due to generation of propagating P and S waves in the bottom layer, absorption of evanescent compressional waves in the bottom, generation and absorption of shear waves in the bottom (Zhang and Tindle, 1993b). Absorption of energy may be included by allowing the wavenumber $k = \frac{\omega}{c(z)}$ to have a small imaginary part α. Attenuation is included in the model by the replacements

$$\frac{\omega}{c_2} \rightarrow \frac{\omega}{c_2} + i\alpha_2, and\ \frac{\omega}{c_s} \rightarrow \frac{\omega}{c_s} + i\alpha_s \qquad (4.15)$$

where $\alpha_2\ and\ \alpha_s$ are the attenuation coefficients of compressional waves and shear waves in the bottom layer, respectively.

5. Simulations and comparison with field data

5.1 Simulations in ideal waveguide

A Matlab program (see Appendix E) was developed based on the theory presented in chapters three and four. The code was first tested employing the case of a Pekeris wave guide with attenuation employing a water depth H = 54 m, sound velocity in water $c_1 = 1500\, m/s$, sound velocity in second medium $c_2 = 1600\, m/s$, density ratio of second to first media $\rho_2/\rho_1 = 1.25$ and attenuation of second medium $\alpha_2 = 3.598 \times 10^{-3}\ dB/m$ at a frequency of 100 Hz, source depth $z_0 = 9\, m$ and receiver depth $z = 10.8\, m$. The normal mode real eigenvalues k_n for the first four modes were calculated the way described in Fig.4.2 and found to be $k_1 = 0.4158535$, $k_2 = 0.4066812$, $k_3 = 0.3918457$ and $k_4 = 0.3658948$

The above choice parameters yields $\frac{\omega}{c_2} = 0.3927$ and only the first two modes are trapped in the sense that the real part of their eigenvalues lie between the upper bound $\frac{\omega}{c_1} = 0.4189$ and the lower bound $\frac{\omega}{c_2} = 0.3927$. If the attenuation is set zero, then the third mode is also trapped. Therefore the introduction of attenuation converts mode three from a trapped mode to a leaky mode (e.g. k_3 changing from 0.391841 to 0.39243).

By using this set of wave number values, the acoustic pressure P(r, z) can be calculated as a function of range employing eq. (3.25) (cf. Fig. 5.1). The figure shows the results of including one, two, three and four modes.

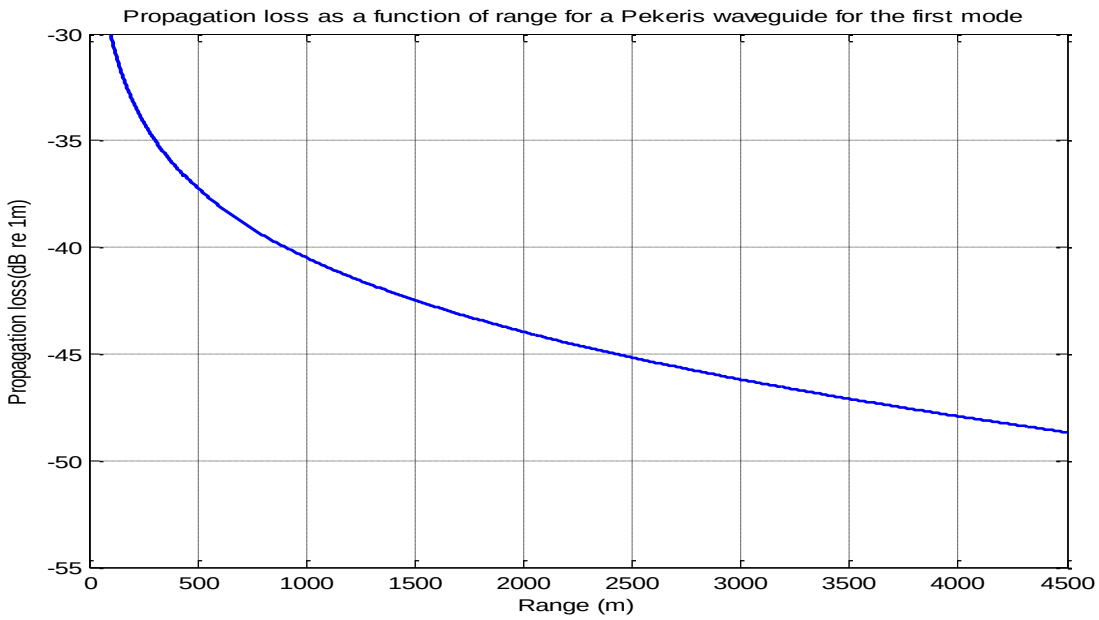
Propagation loss as a function of range for a Pekeris waveguide for the first mode
Propagation loss(dB re 1m)
-30
-35
-40
-45
-50
-55
0
500
1000
1500
2000
2500
3000
3500
4000
4500
Range (m)

(a)

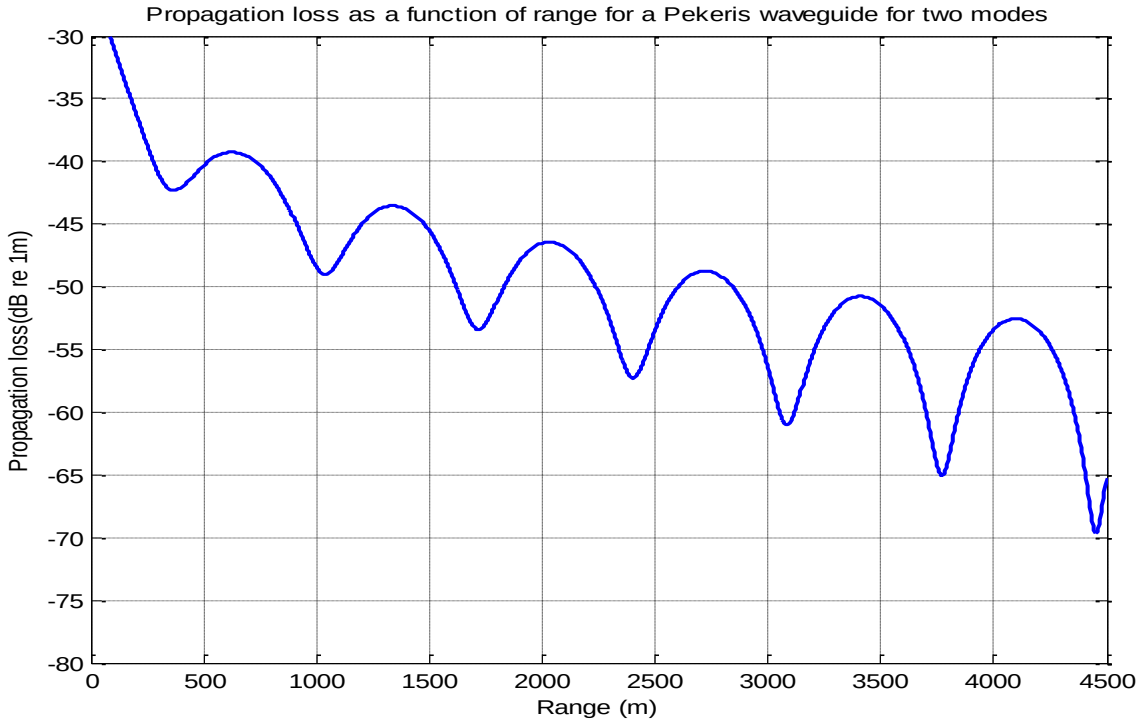
Propagation loss as a function of range for a Pekeris waveguide for two modes
Propagation loss(dB re 1m)
-30
-35
-40
-45
-50
-55
-60
-65
-70
-75
-80
0
500
1000
1500
2000
2500
3000
3500
4000
4500
Range (m)

(b)

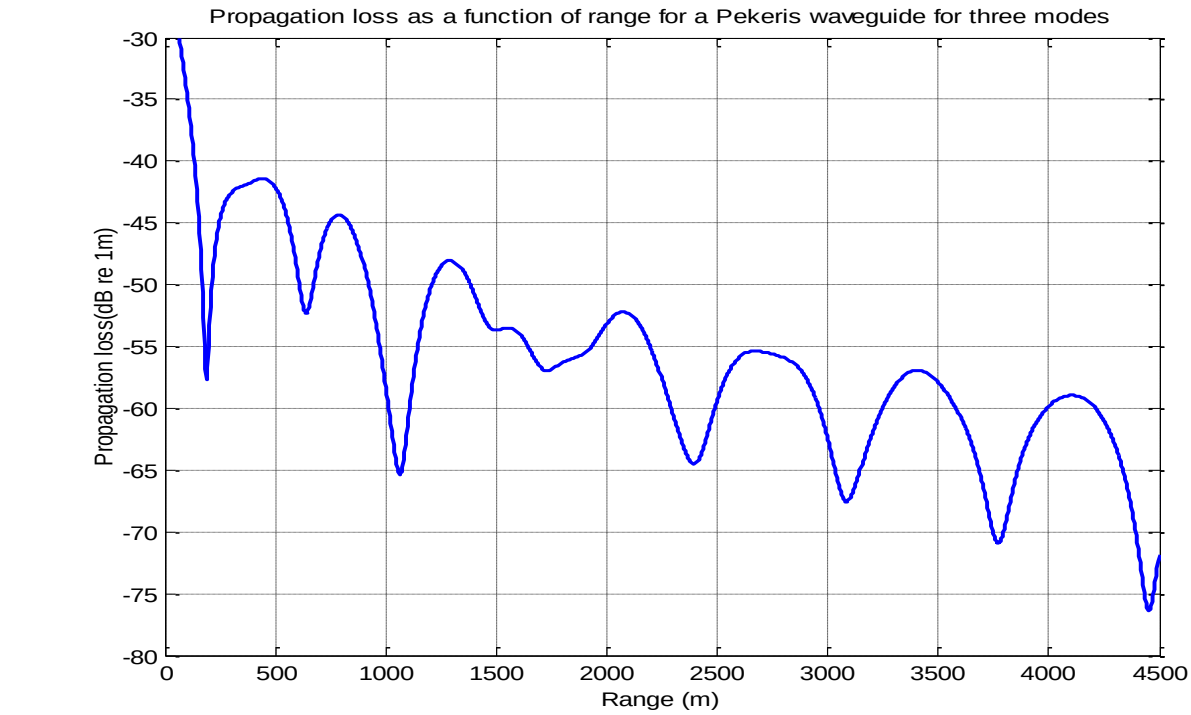

(c)

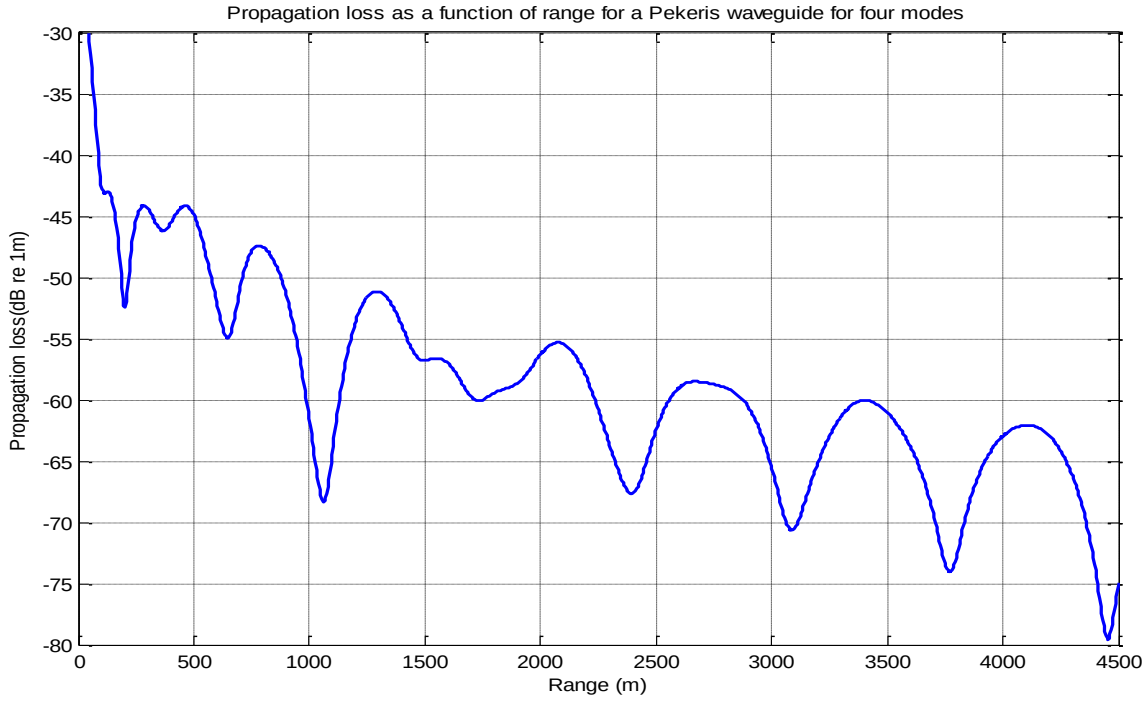

(d)

Figure: 5. 1 Propagation loss as a function of range for a Pekeris waveguide with an attenuation fluid bottom for: (a) mode 1, (b) modes 1-2, (c) modes 1-3, and (d) modes 1-4 respectively.

The result shown in Fig. 5.1d was first obtained by (Zhang and Tindle, 1993a). Since our simulation program gave the same propagation loss curve, it is a good check on the reliability of the code.

Figure 5.2 represents an extension of Fig. 5.1d, where a much larger range is considered (up to 50 km). The propagation loss curve shows resemblance with the curves in Fig. 2.2a.

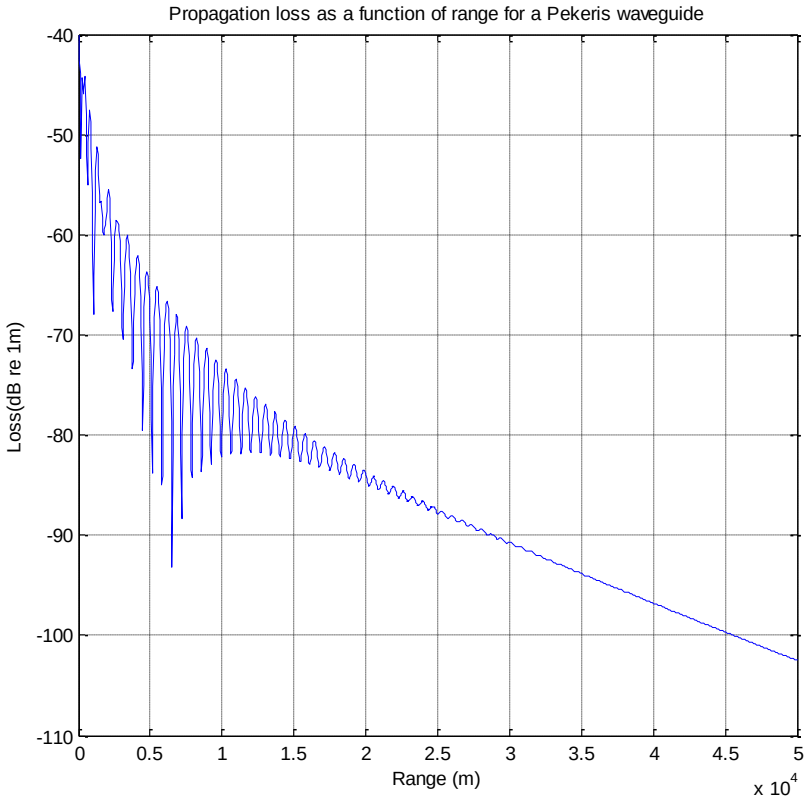

Figure: 5. 2- Propagation loss as a function of range for a Pekeris waveguide with attenuation fluid bottom at large range.

According to Auld (1973), a simple idealized waveguide consists of a homogenous fluid (water) with pressure-release boundary condition at upper and lower interfaces. This boundary condition requires the pressure to vanish at these interfaces.

The normal mode solutions can formally be written on the form P(r, z) = R(r) Z(z) using separation of variables. The eigenfunctions Z(z) for the ideal case must therefore satisfy the boundary conditions:

$$Z(z)\,|_{z=0} = 0 \; and \; Z(z)\,|_{z=H} = 0 \qquad (5.1a)$$

and a possible solution will be

$$Z(z) = sin(\gamma_n z),\ 0 \le Z \le H \tag{5.1b}$$

with an idealized model equation of the form

$$\gamma_n H = n\pi,\ \text{n = mode number} \tag{5.2}$$

where γ_n are eigenvalues. A plot of the eignfunctions (three first modes) of an idealized (pressure - release) waveguide is shown in Fig. 5.3.

In case of a real Pekeris waveguide, eq. (5.2) is replaced by eq. (4.13) (e.g. pressure - release BC at the effective depth He). The eigenfunctions then take the form (Zhang and Tindle, 1993a):

$$\left.\begin{aligned} Z_n(z) &= sin\left(\frac{n\pi z}{He}\right),\ 0 \le z \le H \\ Z_n(z) &= sin\left(\frac{n\pi z}{He}\right)\exp\left[-kn(z-H)\sin\left(\frac{c1}{c2}\right)\sqrt{1-\frac{n^2\pi^2}{kn^2He^2\sin^2(c1/c2)}}\right],\ z > H \end{aligned}\right\} \tag{5.3}$$

where n = $1, 2, 3$

The upper part of eq. (5.3) represents the familiar oscillatory modes in the water column for an idealized (pressure-release) waveguide (Fig.5.3), and the lower part represents the devations from the idealized waveguide determined from a combination of waveguide parameters such as channel depth, density ratio, critical angle and bottom layer attenuation (Buckingham and Giddens, 2005)).

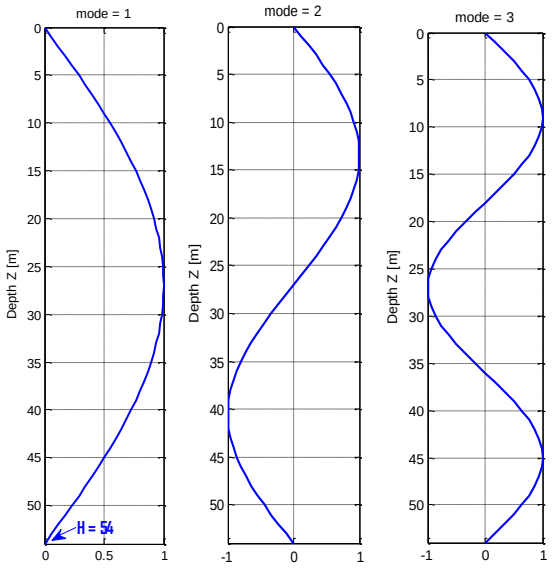

Figure: 5. 3 - Three first eigenfunctions (normal modes) for an idealized waveguide.

Figure 5.4 shows an example of the eigenfunctions (normal modes) for the real Pekeris waveguide calculated from eq. (5.3). In this simulation $H = 54\ m$ and $He \approx 62\ m$.

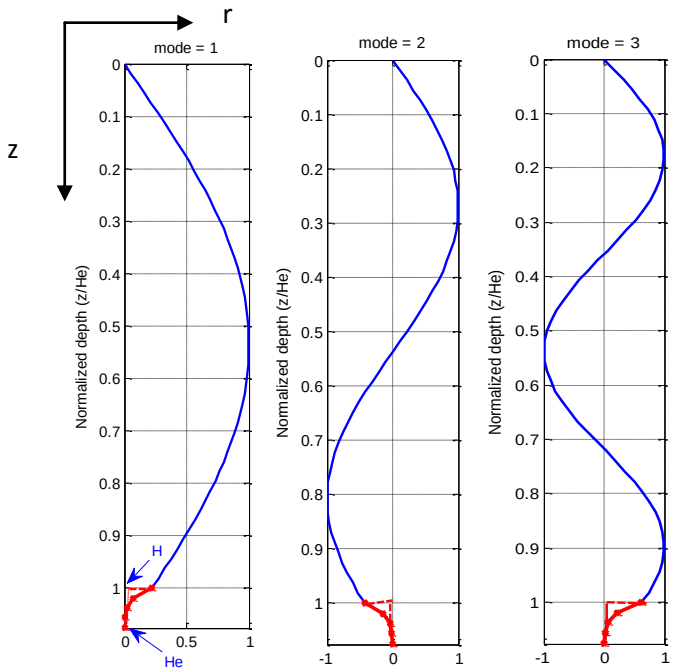

Figure: 5. 4 (a) - Normal modes of the Pekeris waveguide with a depth of H and effective depth of He.

The normal modes of the Pekeris waveguide are sine waves that vanish at the surface and abruptly change to decaying exponentials below the true sea bottom. (e.g. evanescent modes). The attenuation of sound in the sea bottom represents the major loss mechanism in shallow water and is proportional to the area of the decaying mode (labeled with the red in Fig. 5.4).

The propagation of pressure signals in a waveguide exhibits a phenomenon called dispersion, where the different frequency components travel at different velocities. The dispersion is due to the geometry and the physical properties of the waveguide, hence called geometric dispersion (Clay and Medwin, 1977a). As Kragh et al. (2004), stated these modes travel at different phase and group speeds as a function of frequency, and a pulse will disperse as it propagates.

The phase speed is the horizontal propagation speed ($c_n = \omega/k_n$) of a wave front corresponding to a mode, whereas the group speed ($v = d\omega/dk_n$) of a mode represents the speed at which an energy packet propagates down the waveguide. Fig. 5.6 shows plots of phase and group wave velocities for a Pekeris waveguide.

Another important characteristic of Pekeris waveguide is the so called cutoff frequency. It represents the lowest frequency that can propagate in the waveguide. Ewing et al. (1957) derived the following expression for the cutoff frequency for a mode n:

$$f_{cutoff}(n) = (n - 0.5) \times c_1 \times c_2/(H \times \sqrt{(c_2^2 - c_1^2)})/2 \qquad (5.4)$$

Figure 5.5 shows how the cut-off frequency depends on depth and mode number.

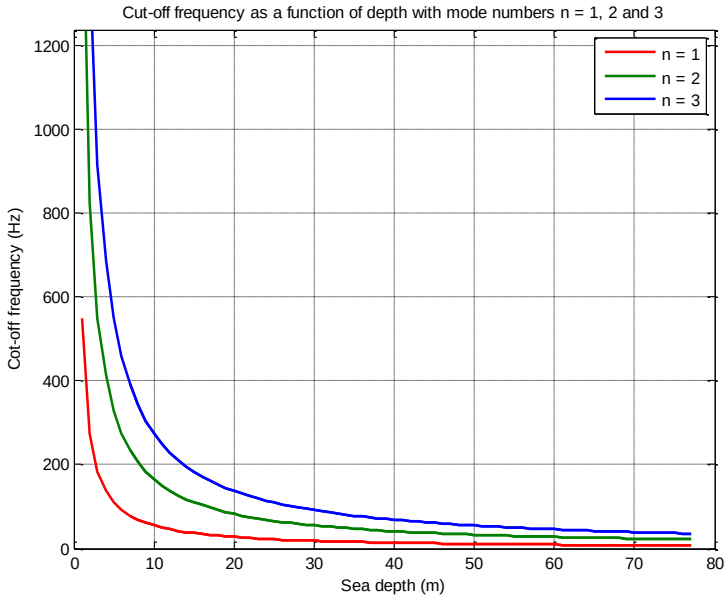

Figure: 5. 5 Cut-off frequency as a function of depth for mode numbers n = 1, 2 and 3. The parameters used are c_1 = 1480 m/s, c_2 = 2000m/s and depth H = 77m.

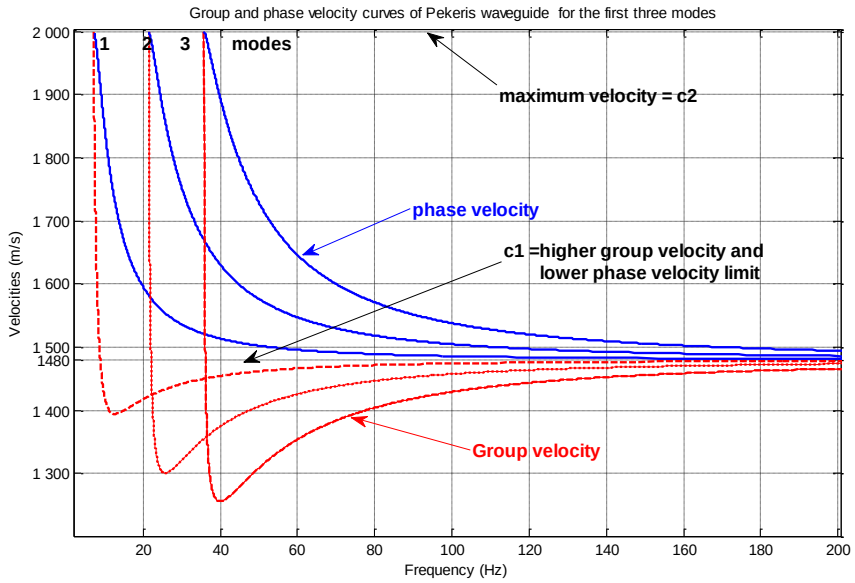

Figure: 5. 6 Phase and group velocities for modes 1, 2, and 3 for the Pekeris waveguide model. The parameters are c_1 = 1480 m/s, $\rho_1 = 1000\frac{kg}{m^3}$, c_2 = 2000m/s and $\rho_2 = 1025\frac{kg}{m^3}$, depth = 77m.

5.2 Waveguide simulation with single source and single receiver-time domain

In this section we present simulations in the time domain. By calculating the normal mode responses over a band of frequencies and using Fourier synthesis, the corresponding time-domain response can be obtained. A Ricker wavelet with a center frequency of 50 Hz was employed. Its amplitude spectrum is shown in Fig. 5.7b. Figure 5.7a gives a sketch of the acquisition geometry employed in the Pekeris waveguide model. Both the source and receivers is placed a depth of 7 m, and the thickness of the water layer is set to 54 m. In the first simulations we assumed that the offset (source - receiver separation) varied between 1 and 50 km. As discussed earlier, the modes generated in a shallow-water waveguide are dispersive. This can be easily seen from Figs. 5.8 a-c. In these simulations we employed the following modal parameters: c_1 = 1500 m/s, c_2 = 1600 m/s and $c_s = \alpha_s = 0$.

(a)

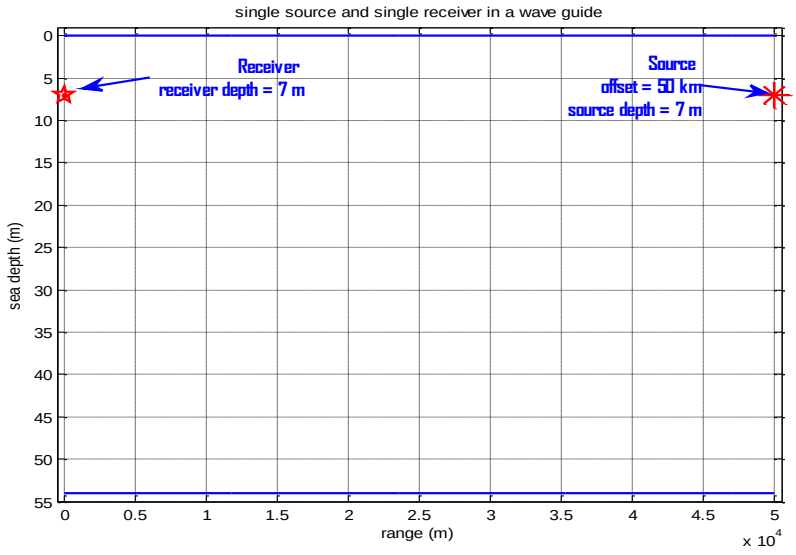

(b)

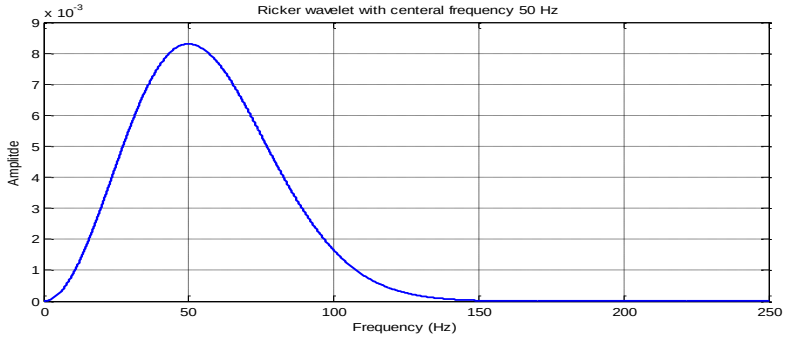

Figure: 5. 7 (a) Schematic diagram of a Pekeris waveguide-model for single source and single receiver where both placed at a depth of 7m and with a separation distance of 50 km. (b) Amplitude spectrum of Ricker wavelet with center frequency of 50 Hz

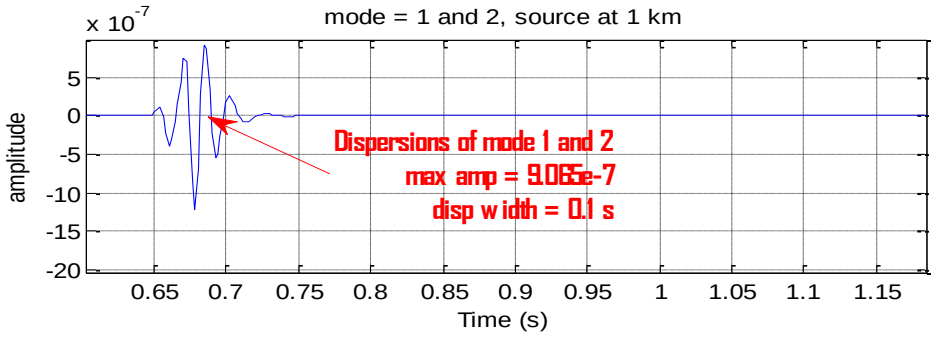

(a)

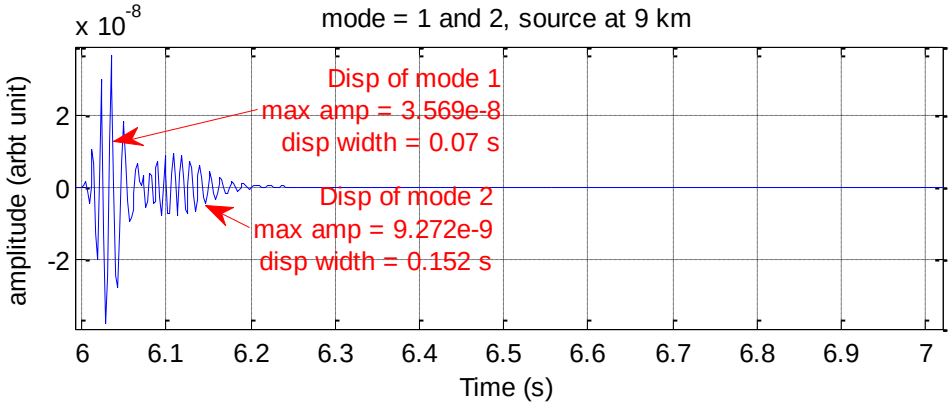

(b)

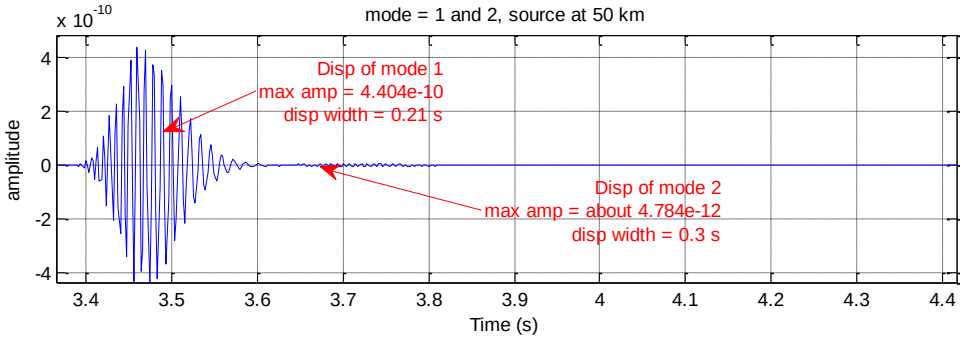

(c)

Figure: 5. 8 Simulation of the dispersive modes for an offset of (a) 1 km, (b) 9 km (c) 50 km. Modes n = 1 and n = 2.

In the previous example a fluid-like sea bottom was assumed, and also a small velocity constant. We now consider a more realistic case of a stronger constant and also investigate the effect of including a solid bottom with shear characteristics. In the simulations we assumed an offset of 9 km, c_1 = 1480m/s, c_2 = 2000m/s. Figure 5.9a shows the two first modes assuming a solid and attenuating sea bottom with $c_s = 200\, m/s$ and $\alpha_s = 0.2$, whereas Fig. 5.9b shows the same two modes in case of a fluid-type bottom (e.g. $c_s = \alpha_s = 0$). Direct comparison shows that an attenuating sea bottom reduces the total duration length of the two

modes (and also slightly reduces the peak amplitude). Also by comparing Figs. 5.8b and 5.9b, we can see that a stronger contrast enhances the buildup of the modes as expected (stronger reverberations that can add constructively).

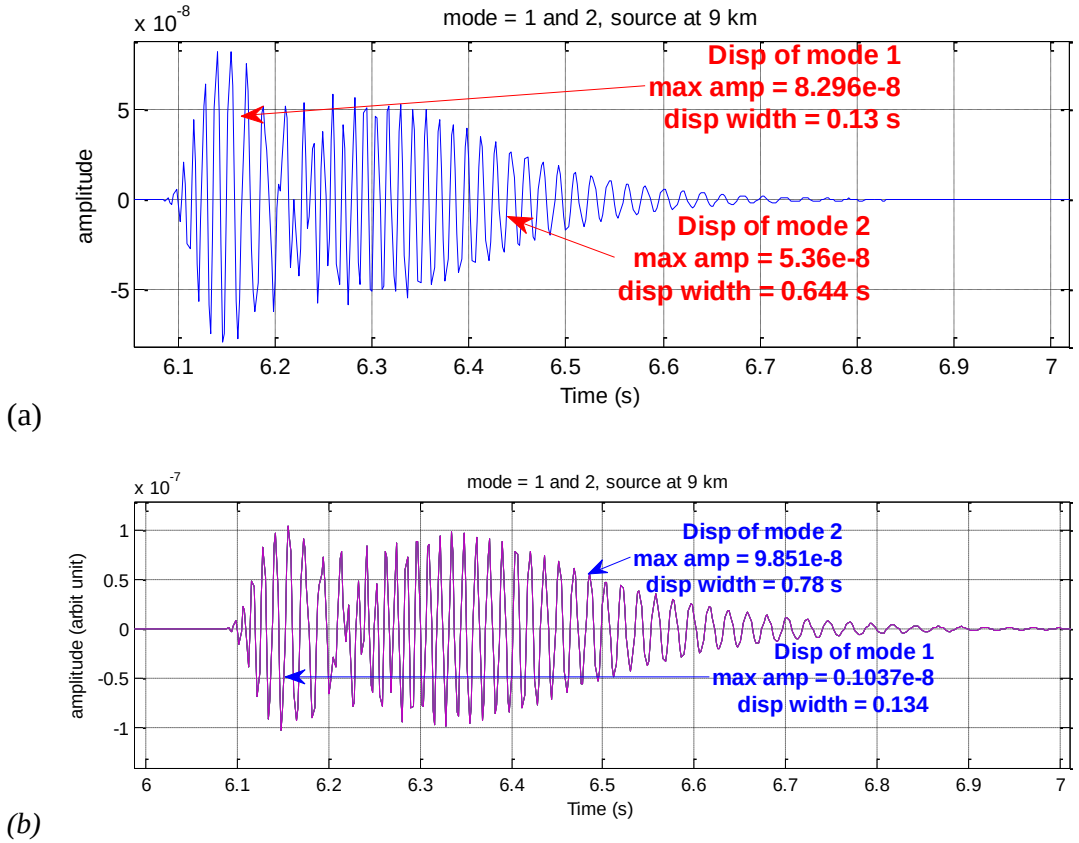

Figure: 5. 9 Dispersive modes (1 and 2) for an offset of 9 km. (a) Attenuating sea bottom and (b) fluid like sea bottom.

5.3 Waveguide simulation with variable-depth-streamer-time domain

Recent studies by Soubaras et al. (2012b) and (2013) have demonstrated that the variable-depth-streamer acquisition is an effective de-ghosting technique and can extend the usable primary bandwidth in both the shallow and deeper parts of the seismic section (with low frequencies down to 2.5 Hz and high frequencies up to 160Hz, and when combined with source de-ghosting, this has been extended to 200 Hz) (Sablon et al., 2012). Some of the main characteristics of the slanted streamer are:

- good signal-to-noise ratio, especially at low frequencies

- benefit in the imaging of deep targets and challenging environments due to the improved low-frequency response of the hydrophones and reduced sea-state noise level at currently considered as extreme depths (up to 50 m) (Sablon et al., 2012).
- allows recording of a wide diversity of receiver ghosts, particularly for shallow events, and after summing the response along the cable, can be tuned to provide the maximum possible bandwidth for a given geological setting and water depth (Sablon et al., 2012).

In general, as the cable is moved deeper, an improved low frequency response is obtained as well as a lower noise level (Soubaras and Dowle, 2010). However, the streamer does not follow variable-depth profile over its entire length. Usually, it can be divided in two sections where the first section is curved while the second one is flat.

In our simulations we used the following parametric equations to describe this shape:

$$\left.\begin{aligned} z(x) &= z_0 + s_0 x\left(1 - \frac{x}{2x_c}\right), for\ x \le x_c\ \ and \\ z(x) &= z_0 + s_0\left(\frac{x_c}{2}\right) \quad , for\ x > x_c \end{aligned}\right\} \tag{5.5}$$

with depth along Z-axis and offset along X-axis. The upper equation provides the curved profile along the varying depth while the lower equation provides a straight line (constant depth). In eq. (5.5) typical values will be z_0= 6 m (initial depth), $s_0 = 0.02$ (slope of initial part of the streamer) and $x_c = 4400m$, Figure 5.10 shows a schematic illustration of a variable-depth streamer.

In the following examples of mode computation for a stated streamer with parameters as above, will be given. Figure 5.11 shows a sketch of the acquisition geometry for the Pekeris waveguide model. In all simulations the source is placed at a depth of 9.8 m. the first set simulations shows a subset of the actual data, e.g. the recording of the shallowest receiver for two different offsets of 9 km and 50 km, respectively. (cf. Figs. 5.12 a and b). Figure 5.12 shows both the two first modes in the time-domain accompanied with the corresponding amplitude spectrum. The largest offset corresponds to the largest signal duration as expected, and also a higher degree of interference also reflected in the spectrum.

In these simulations we employed the following model parameters: c_1 = 1500 m/s, $\rho_1 = 1000\ kg/m^3$, c_2 = 1600m/s , $\rho_2 = 1025\ kg/m^3$, H = 77m (e.g. fluid like sea bottom).

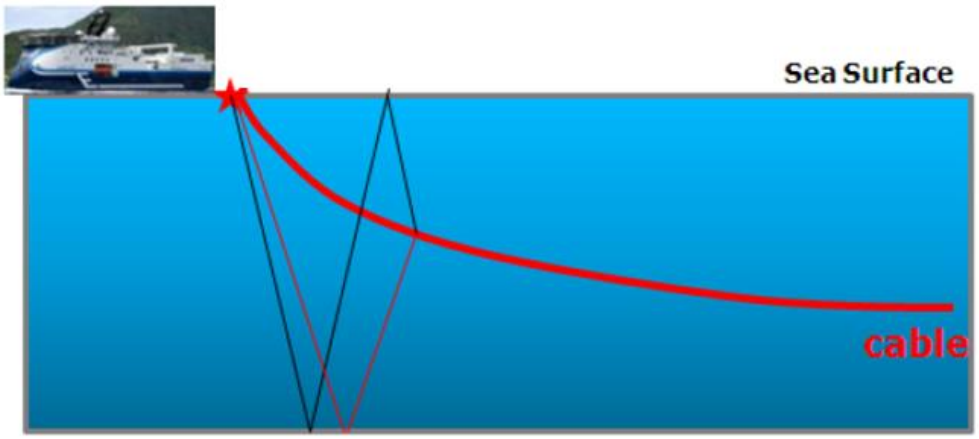

Figure: 5. 10 Schematic illustration of a variable-depth streamer adapted from Soubaras et al. (2012b).

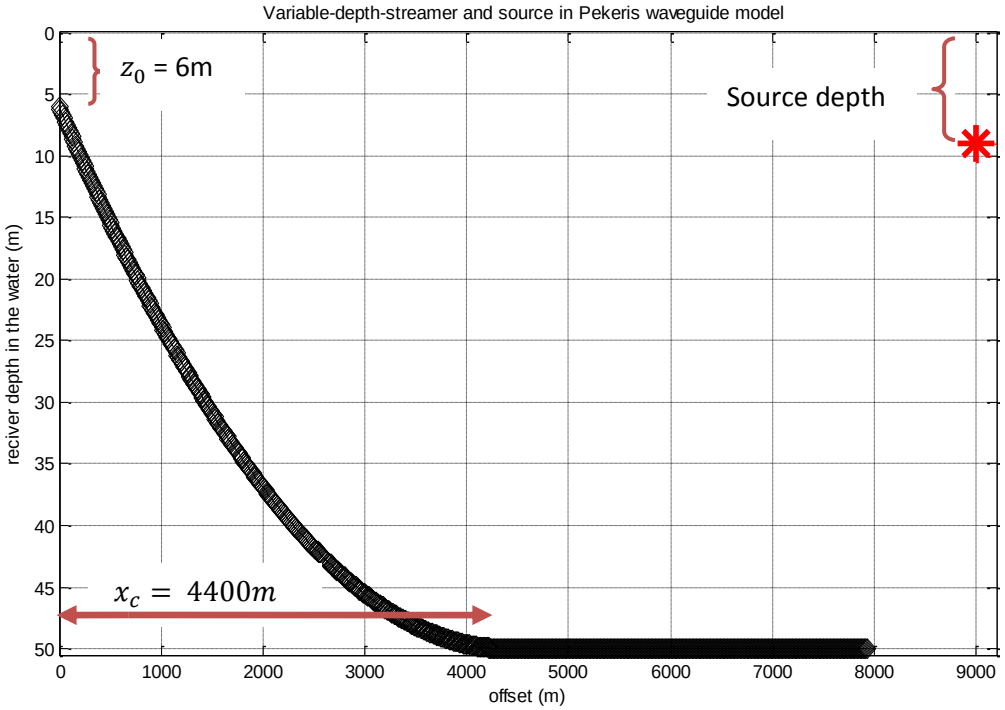

Figure: 5. 11- Simulation of Variable-depth streamer and single source in Pekeris waveguide model.

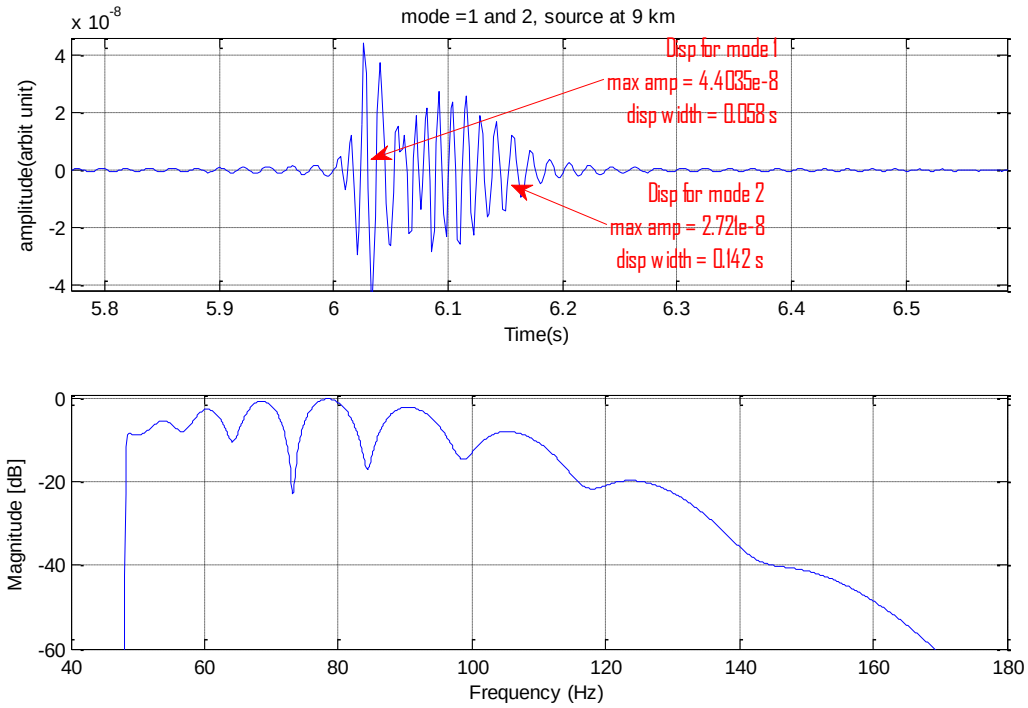

(a)

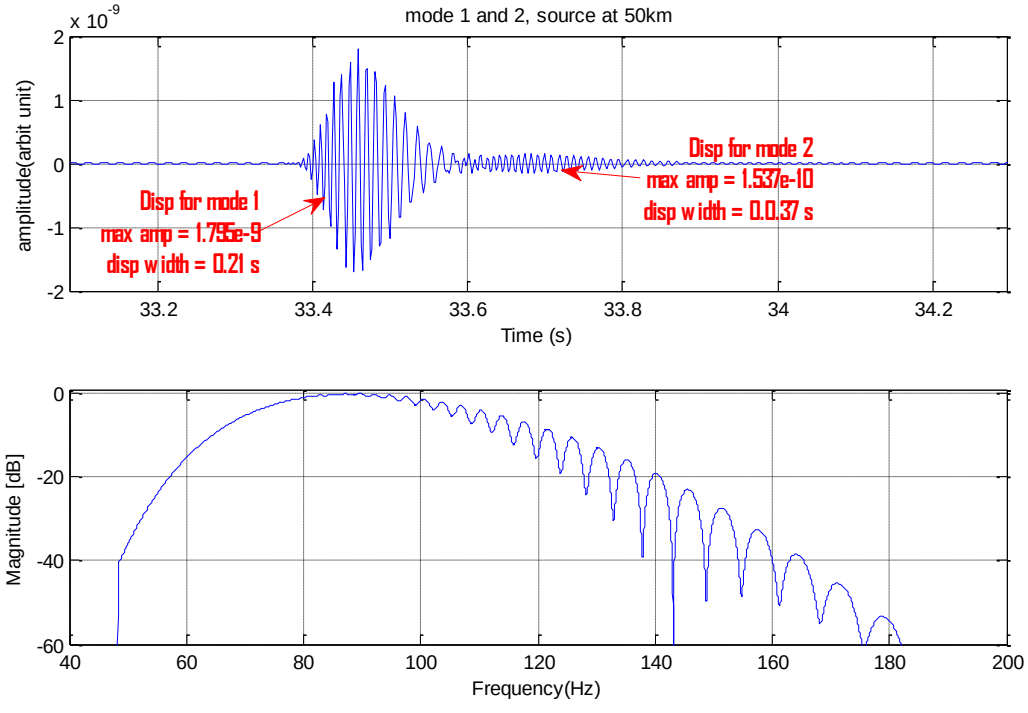

(b)

Figure: 5. 12- Simulation of the dispersive modes 1 and 2 in Pekeris waveguide measured at the most shallow receiver (a) 9km and (b) 50 km offset.

By carrying out a series of such computations as in Fig. 5.12, we can calculate how the maximum amplitude varies with offset for each of the two modes (cf. fig. 5.13a). In addition we can calculate how the dispersion time-width changes with offset for the same two modes (cf. fig. 5.13b). The amplitude characteristic is of an exponential type and reaches a plateau

after about an offset of 35 km, but the dispersion time width seems to increase more or less steadily with increasing offset.

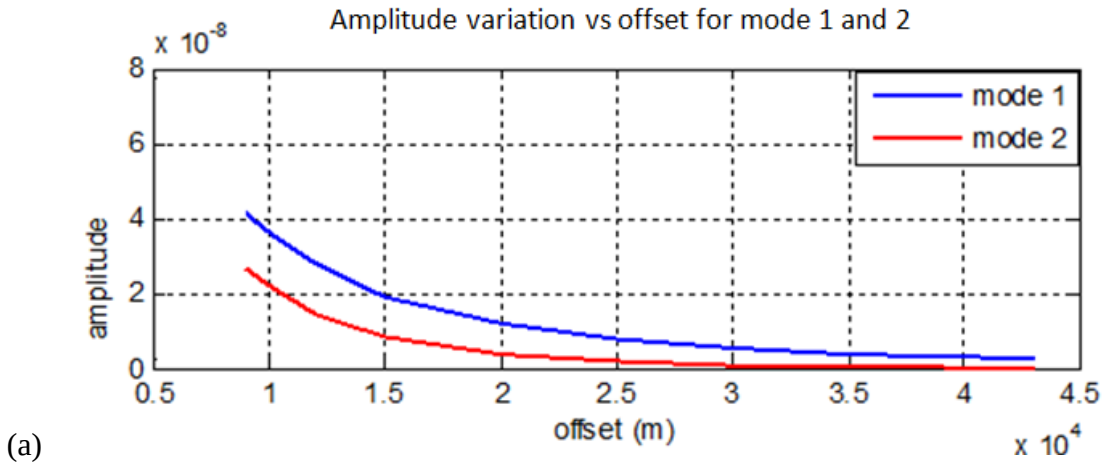

(a)

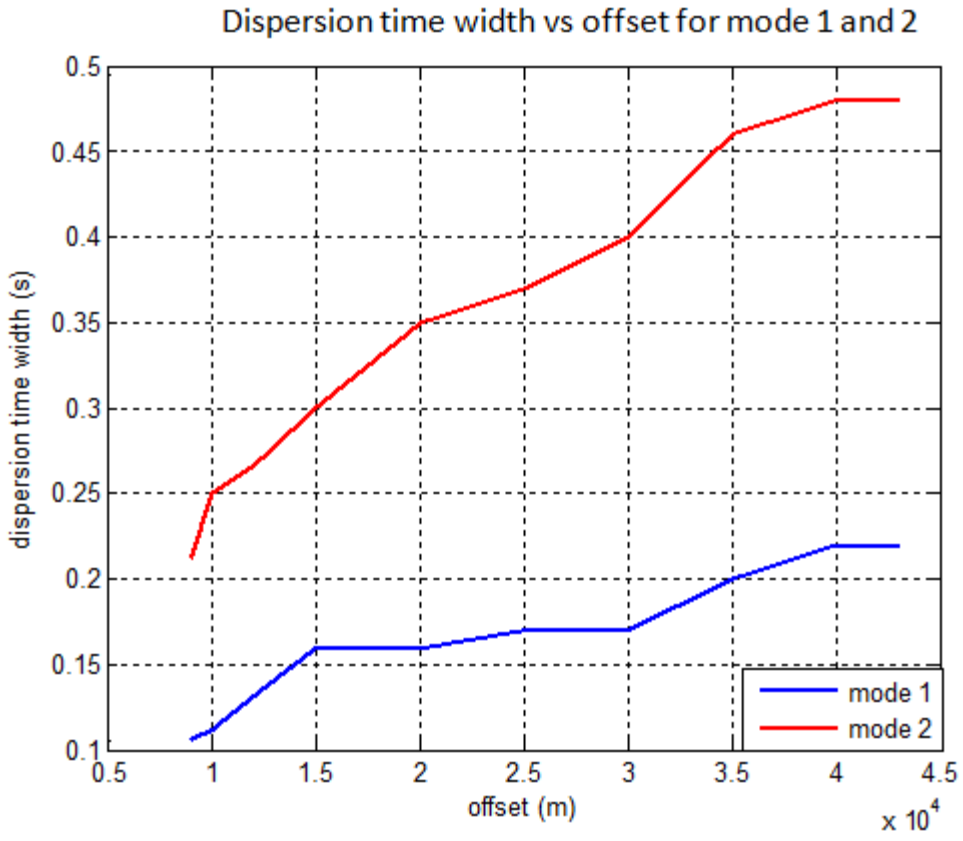

(b)

Figure: 5. 13- (a) Amplitude variation with offset for modes 1 and 2 (b) Variation in dispersion time width with offset for modes 1 and 2 separattly.

In case of a single source at fixed position, we can also compute how the received maximum amplitude varies along the variable-depth streamer. Figure 5.14 shows such an example of amplitude variation versus (range coordinate) of receiver. As in the other cases, the overall

shape of this determined from a set of mechanisms including geometrical spreading, dispersion effects and the properties of the Pekeris waveguide model.

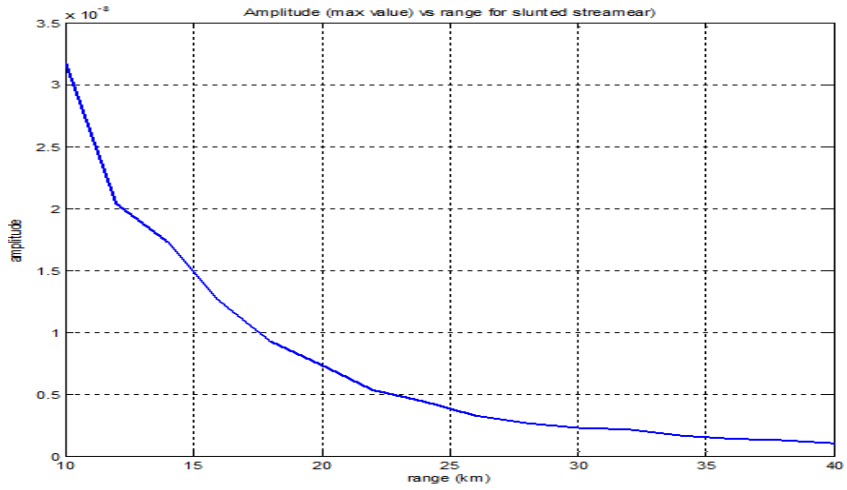

Figure: 5. 14 Amplitude (max value) variation along slanted streamer.

In the situations up to now, we have used a Ricker wavelet with center frequency of 50 Hz. To support the result in Fig. 5.14, we can also calculate a similar response for each individual frequency component. Such a plot is shown in Fig. 5.15, but with the energy or amplitude square used here (dB scale). It can easily be seen how the signal is weakened when the more distant receivers are considered.

To conclude this subsection, we show typical time-records of the shallow-water waves recorded along the slanted streamer, in case of an offset of respectively, 12.8 km and 50 km (cf. Fig.5.16). Offset means here the lateral distance between the source and the shallowest receiver. From Fig. 5.15 we can easily see the dispersive wave character.

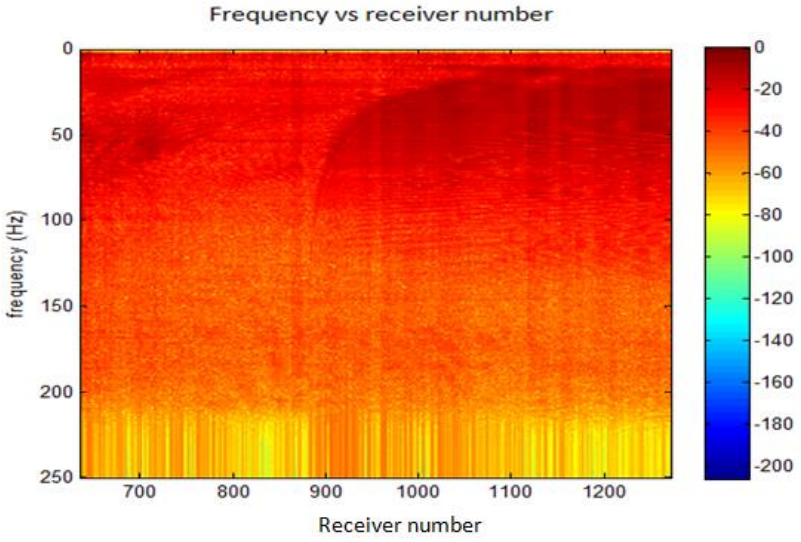

Figure: 5. 15- Frequency-receiver number cross plot of energy

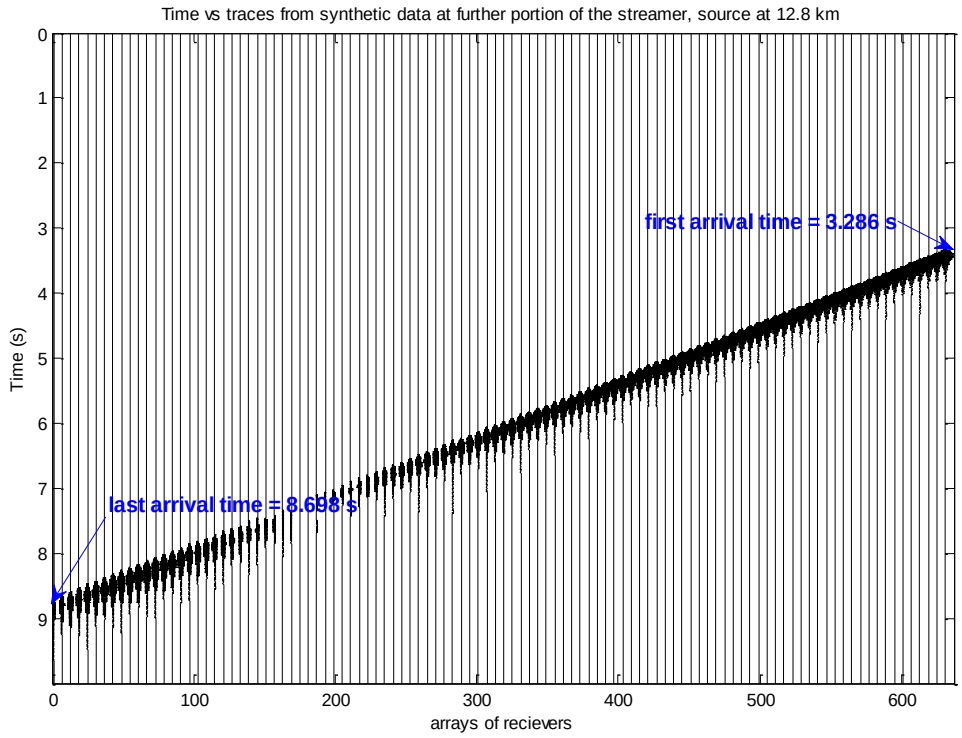

(a)

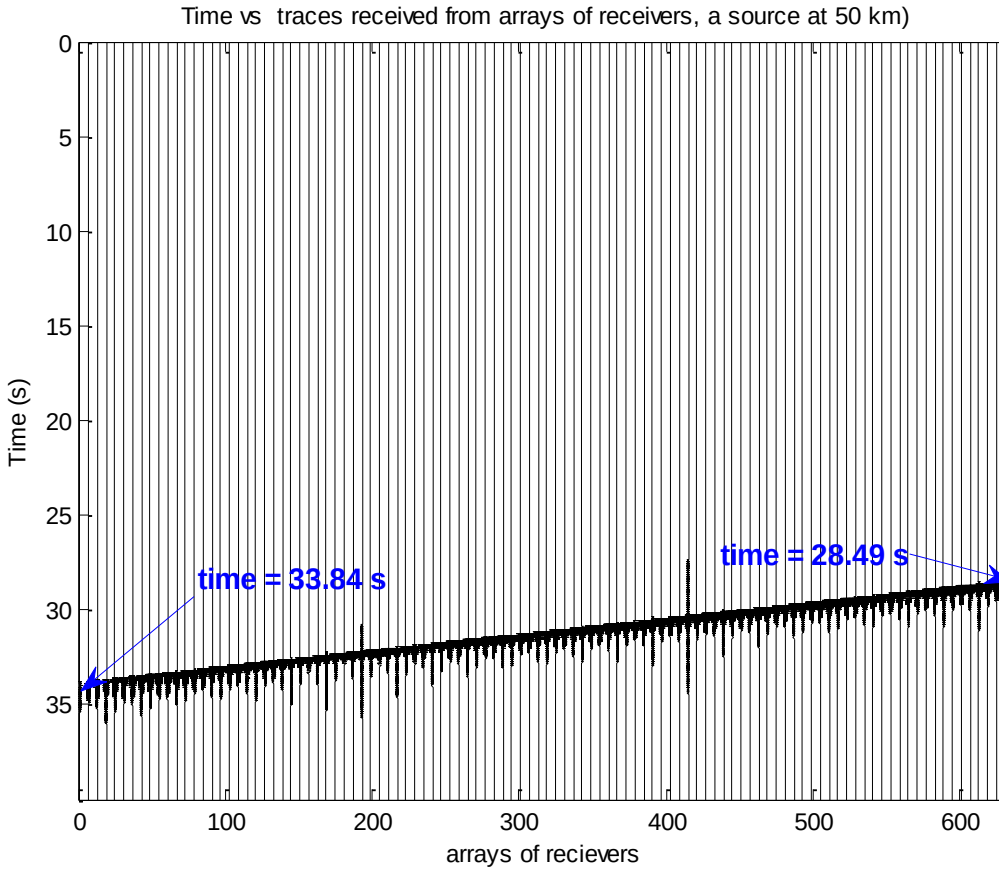

(b)

Figure: 5. 16- Simulation of signals received along slanted streamer for (a) 12.8 km and (b) 50 km offset

5.4 Real data analysis

2D gathers of passive noise recordings were taken from a site in North Sea with a total of 41 shot gathers available.

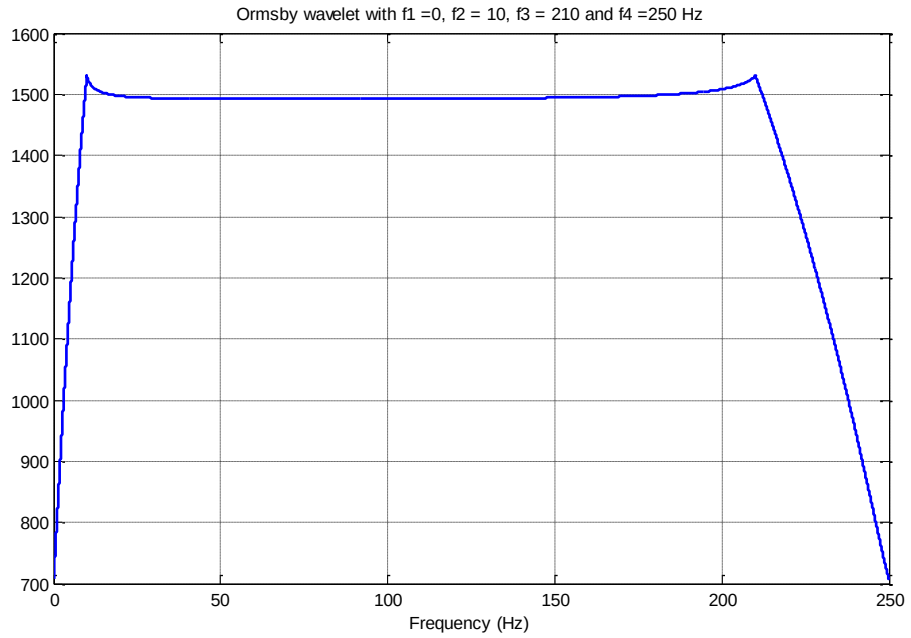

Figure: 5. 17- Amplitude spectrum of Ormsby wavelet

The collection of data was examined carefully before a small subset was chosen for further analysis and comparison with numerical simulations. In order to generate band-limited seismograms an Ormsby wavelet was employed due to its minimum -phase characteristics. Its amplitude spectrum is shown in fig. 5.17. The noise records selected show a high-degree of seismic interference (SI) noise. This type of noise originates from other marine seismic crews surveying the same area. Figures 5.18a and b show examples of SI noise extracted from our data set. In fig. 5.18a one dominant direction can be seen, where as in Fig. 5.18b the interface of two dominant directions of SI can be observed. The dispersive character of the SI noise can be easily seen.

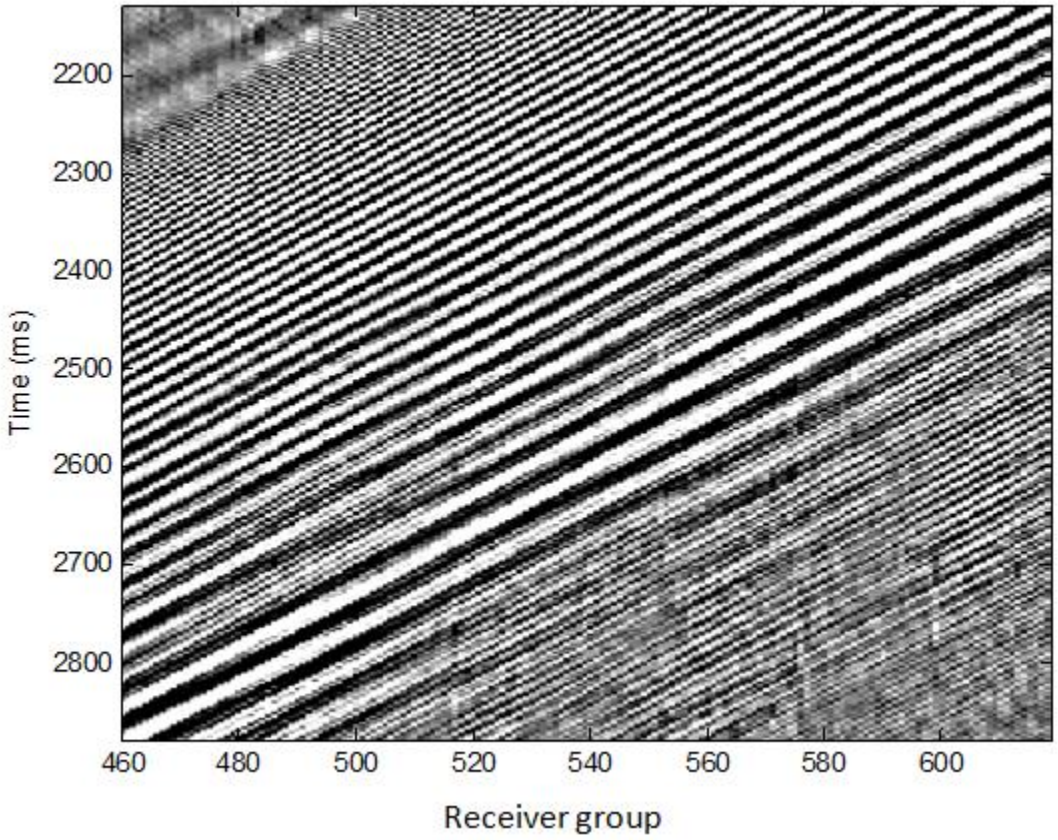

(a)

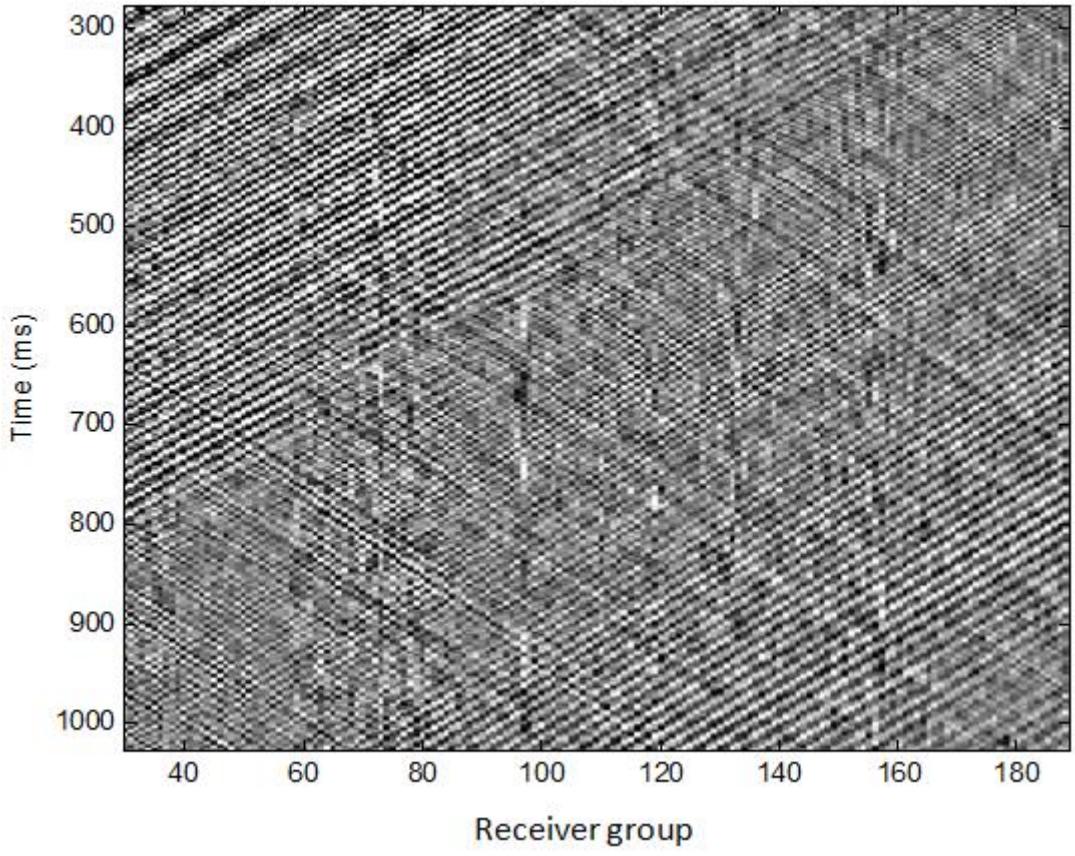

(b)

Figure: 5. 18- Example of SI noise (a) one dominant direction and (b) multiple directions (interference).

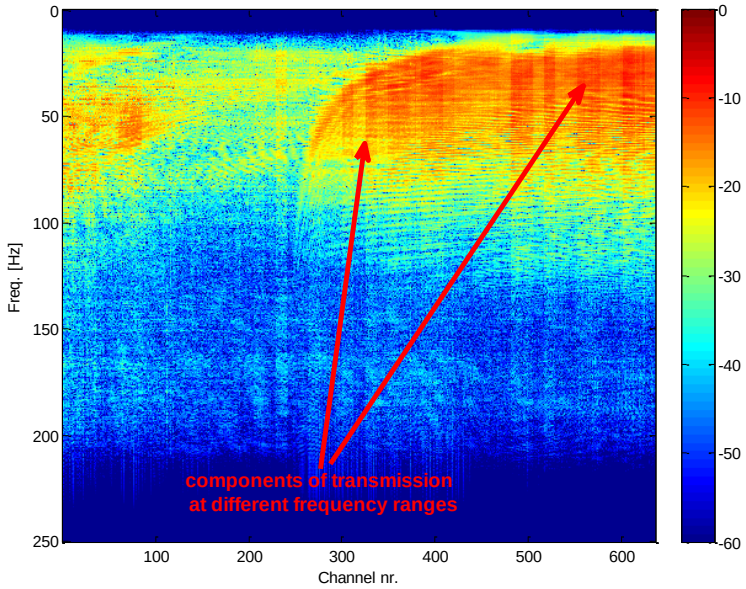

Figure: 5. 19 Amplitud spectrum of slanted streamer recording of SI

To further analysis the SI noise, the amplitude spectrum of the time-recording of each receiver was calculated and combined in a 2D plot as shown in Fig. 5.19. The dispersive character can easily be seen. Also after a spatial Fourier transform along the range coordinate of the receivers, an *f-k* plot was computed as shown in Fig. 5.20. Except from distortions due to aliasing, the dispersive character of the waveguide is reflected in the plot and with the higher frequencies significantly more attenuated than the lower ones. In this case, frequencies above about 100 Hz seem to be associated with negligible energy.

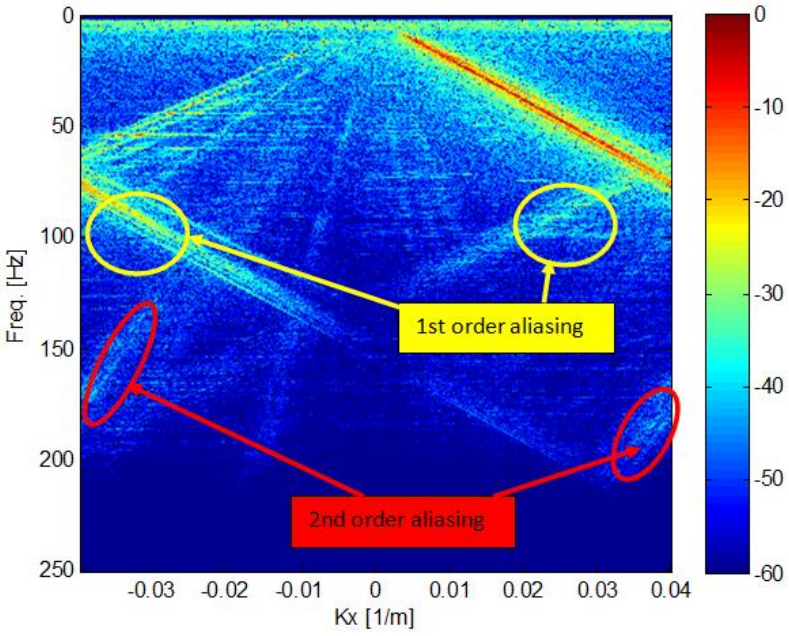

Figure: 5. 20 – F-k spectrum of slanted-streamer recording of SI.

5.5 Comparison between simulated and real data

In sea water the acoustic wave velocity varies typically between 1450 m/s and 1500 m/s depending on pressure, salinity, and temperature. In water-saturated sediments, (where velocity is proportional to the interstitial water sound speed), the sound velocity ranges typically between 1500 – 2000 m/s (Lurton, 2002). For our simulations we considered the following parameters: c_1 = 1480 m/s, $\rho_2/\rho_1 = 1.25$, c_2 = 2000m/s, H = 77m, $c_s = 200\, m/s$ and $\alpha_s = 0.2$.

We selected the real data time recording of SI shown in Fig.5.21b. The first arrival time of the nearest receiver is about 3.374 s. By adjusting the offset during simulation to 12.8 km, the synthetic time recording shown in Fig. 5.21a was obtained. The most striking difference between these two data sets is the time duration. We will discuss this more in the concluding chapter. To be able to compare the real and simulated data in a better way, zoomed versions were employed as shown in Figs. 5.22 a and b (selected subset of receivers). We can see that both the real and simulated data are of dispersive character with similar main periodicity. However, in case of the field data, a much longer recording exists with a higher degree of complexity.

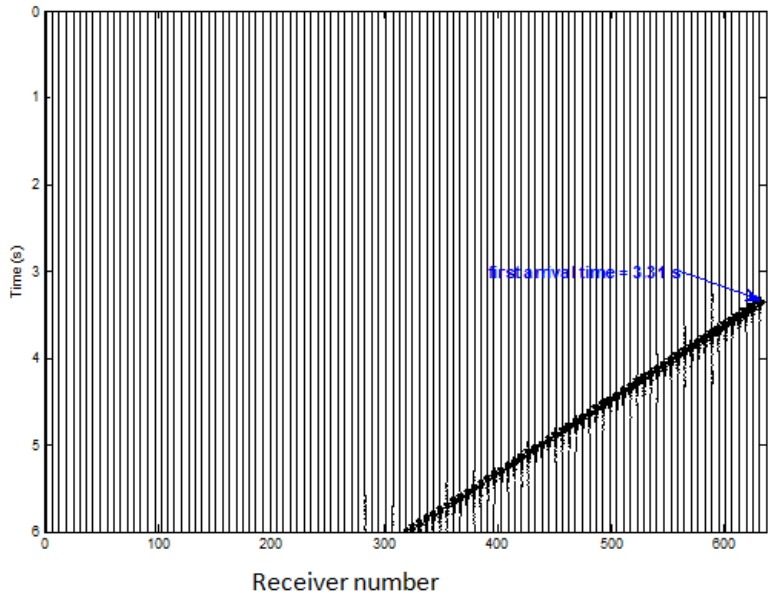

(a)

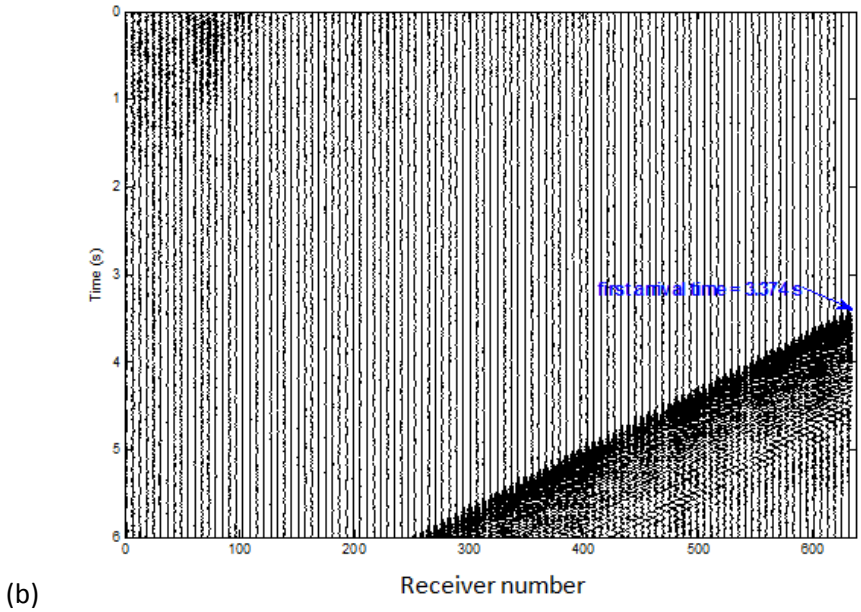

Figure: 5. 21- Time recording: (a) synthetic data and (b) real data from slanted streamer

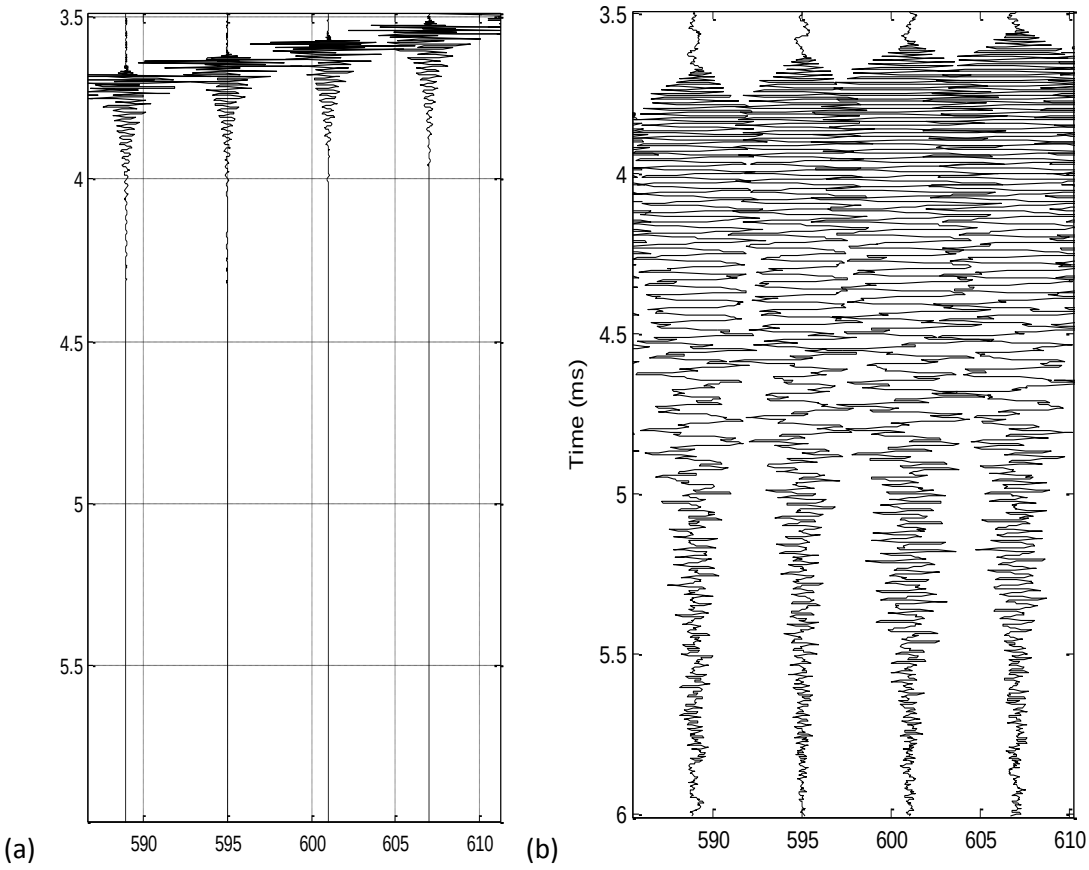

Figure: 5. 22- Zoomed versions of the results in Fig. 5.21 (a) synthetic data and (b) field data

Figs. 23a and b show amplitude- time history and corresponding frequency spectrum for (a) modeled case in a Pekeris waveguide and (b) real data recorded in North Sea. In both cases a fixed receiver along the slanted streamer is considered. On comparison, the field data look

much more dispersive. Figure 5.24 shows the amplitude- time history and frequency spectrum in case of multiple sources output from the modeling program.

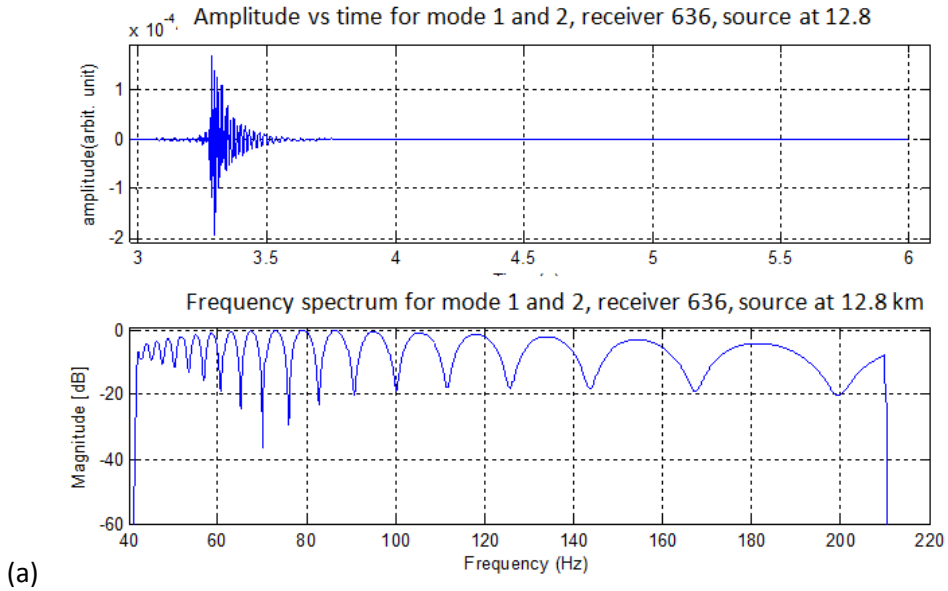

(a)

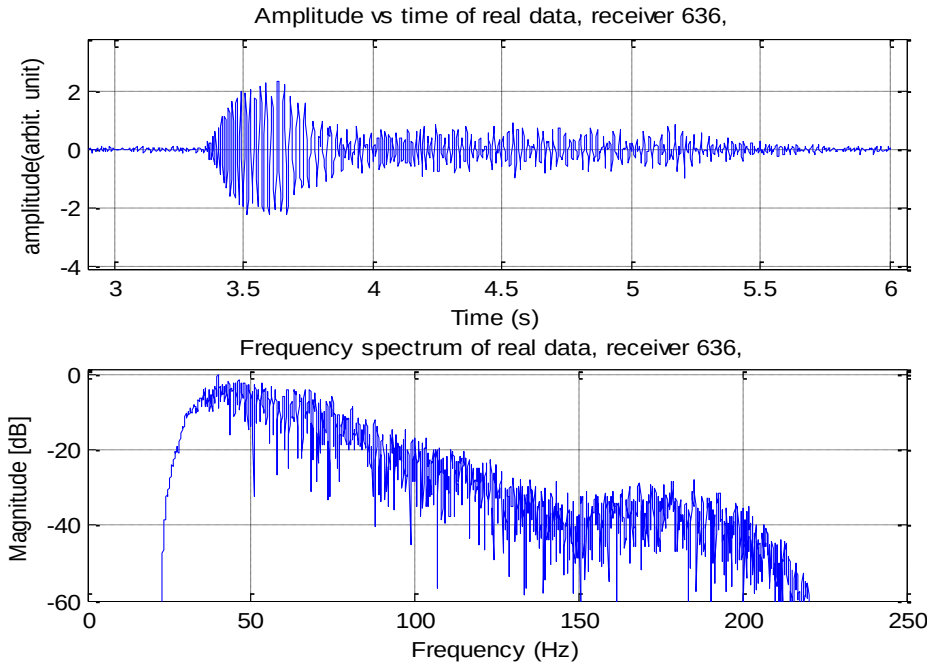

(b)

Figure: 5. 23- Amplitude vs time and frequency spectrum for (a) simulated data and (b) real data

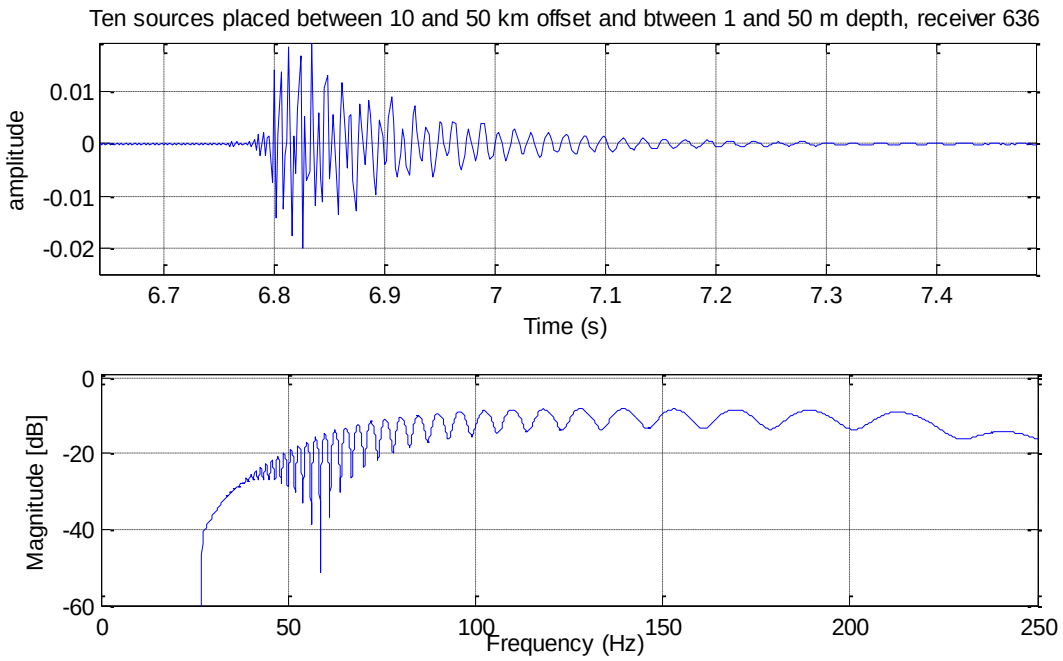

Figure: 5. 24- *Amplitude vs time and frequency spectrum in case of multiple sources.*

6. Discussion and conclusions

A Matlab code has been developed to simulate acoustic modes in shallow water. Based on the work carried out in this thesis project, the following main observations can be made from the simulations employing this code:

- The rate of dispersion and also attenuation of the waves in the waveguide depends on the mode number, with the transmission loss increasing both with mode number and range.
- The lower order modes usually travel faster than the higher order modes.
- The characteristics of the wave propagation in the waveguide depend on a series of parameters like temperature, salinity, pressure, depth, contrast, and type of sea bottom (fluid-like or solid-like).
- The energy of the modes travel with the group velocity. Both group and phase velocities decrease with increasing mode number.
- A cut-off frequency exists, which represents the lowest frequency that can propagate inside the waveguide.

In this thesis work we also compared simulated data with field recordings of SI noise in case of a slanted-streamer. The purpose of this investigation was to improve the basic understanding of the propagating mechanisms behind seismic interference noise. It was shown that the real noise recordings locally looked similar to the simulated data. Thus, indicating that SI noise show close resemblance with dispersive modes. However, one main difference exists between simulated and recorded data; the latter has much longer time duration. Possible explanations of several factors including:

- source side (air-gun array) is not represented properly by a single point source, but a more distributed source system of varying strength, and
- due to difference in salinity and temperature the water column is not homogeneous but can be regarded as laminated implies an improved modelling should not use a single homogeneous waveguide model but multiple waveguides.

Future work within SI noise characterization should be based on field records with additional information like location of other vessels (sources) creating the noise and more precise parameters defining the water layer and the sea bottom. Such improved information may lead to more reliable simulations. If not available, an inversion approach could be possibly

employed to identify optional parameters based on the observations. Medwin and Clay (1998) and Bucker (1976) proposed matched field algorithms where the recorded pressure is compared with simulations from a source using a set of trial ranges and depths.

7. References

AULD, B. A. 1973. *Acoustic fields and waves in solids,* New York, Wiley.

BRECHOVSKICH, L. M. & GODIN, O. A. 1999. *Acoustics of layered media,* Berlin, Springer.

BRECHOVSKICH, L. M. & LYSANOV, J. 2003. *Fundamentals of ocean acoustics,* New York, AIP Press.

BRECHOVSKICH, L. M. & LYSANOV, Y. P. 1991. *Fundamentals of ocean acoustics,* Berlin, Springer-Verlag.

BUCKER, H. P. 1976. Use of calculated sound fields and matched-field detection to locate sound sources in shallow water. *The Journal of the Acoustical Society of America,* 59**,** 368-373.

BUCKINGHAM, M. J. 1992. *Ocean-acoustic propagation models,* EUR-OP.

BUCKINGHAM, M. J. & GIDDENS, E. M. 2005. On the acoustic field in a Pekeris waveguide with attenuation in the bottom half-space. 119**,** 20.

CHAPMAN, D. F. & WARD, P. D. 1989. The normal-mode theory of air-to-water sound transmission in the ocean. *J. Acoust. Soc. Am,* 87**,** 18.

CLAY, C. S. & MEDWIN, H. 1977a. *Acoustical Oceanography,* New York, John Wiley & Sons.

CLAY, C. S. & MEDWIN, H. 1977b. *Acoustical oceanography: principles and applications,* New York, Wiley.

COSTA, E. D. S., MEDEIROS, E. B. & FILARDI, J. B. C. 2013. *Modeling and Measurement Methods for Acoustic Waves and for Acoustic Microdevices,* nTech, nTech.

ELLIS, D. D. & CHAPMAN, D. M. F. 1985. *A simple shallow water propagation model including shear wave effects* [Online]. [Accessed 6 78].

EWING, W. M., JARDETZKY, W. S. & PRESS, F. 1957. *Elastic waves in layered media,* New York, The Observatory.

FILIPPI, P. 1999. *Acoustics: basic physics, theory, and methods,* San Diego, Academic Press.

HILL, D., BACON, J., BRICE, T., COMBEE, L., KOENINGER, C., LEATHARD, M. & STEPHEN MCHUGO. 2007. *Over/Under Deghosting: The Practical Aspects of Acquisition and Data Processing* [Online]. Houston, Texas: Offshore Technology Conference

JENSEN, F. B., KUPERMAN, W. A., PORTER, M. B. & SCHMIDT, H. 1994. *Computational Ocean Acoustics,* New York, NY, Springer New York.

KACNEL'SON, B. G. & PETNIKOV, V. G. 2002. *Shallow-water acoustics*, London, Springer.

KATSNELSON, B. G. & PETNIKOV, V. G. 2002. *Shallow water acoustics*, Springer.

KRAGH, E., ROBERTSSON, J., LAWS, R., AMUNDSEN, L., RØSTEN, T., DAVIES, T., ZEROUK, K. & STRUDLEY, A. 2004. Rough-sea deghosting using wave heights derived from low-frequency pressure recordings — A case study Read More: http://library.seg.org/doi/abs/10.1190/1.1851107. 4.

KUMAR, T. P. 1999. *A STUDY ON THE GEOACOUSTIC PROPERTIES OF MARINE SEDIMENTS.* Degree of Doctor of Philosophy In partial fulfilment of the requirements for the degree of Doctor of Philosophy, Cochin University of Science and Technology.

LURTON, X. 2002. *An introduction to underwater acoustics: principles and applications*, Springer.

MEDWIN, H. & CLAY, C. S. 1998. *Fundamentals of acoustical oceanography*, Boston, Academic Press.

ORJI, O. C. 2012. Sea Surface Wave Height Estimation from Dual-Sensor Towed Streamer. 89.

PRESS, F. & EWING, M. 1950. Propagation of explosive sound in a liquid layer overlying a semi-infinite elastic solid. *Geophysics,* 15**,** 426-446.

ROSS, D. 1987. *Mechanics of underwater noise*, Los Altos, Calif., Peninsula Publishing.

RYTOV, S. M., KRAVTSOV, Y. A. & TATARSKII, V. I. 1988. Principles of statistical radiophysics 2. Correlation theory of random processes. *Principles of statistical radiophysics 2. Correlation theory of random processes.. SM Rytov, Yu. A. Kravtsov, VI Tatarskii. Springer-Verlag, Berlin, FR Germany. 10+ 234 pp. Price DM 148.00, US $79.00 (1988). ISBN 3-540-16186-4 (FR Germany), ISBN 0-387-16186-4 (USA).* 1.

SABLON, R., YVES LAFET, LIN, D. & R, S. 2012. Challenges and benefits of variable-depth streamer: from acquisition to interpretation. sep, 2012 ed.

SOUBARAS, R. & DOWLE, R. December 2010 2010. *RE: Variable-depth streamer – a broadband marine solution.*

SOUBARAS, R., DOWLE, R. & SABLON, R. 2012a. BroadSeis: Enhancing interpretation and inversion with broadband marine seismic. 6.

SOUBARAS, R., DOWLE, R. & SABLON, R. 2012b. Variable Depth Streamer Acquisition: Enhancing interpretation with broadband marine seismic. *CSEG RECORDER*.

SOUBARAS, R. & LAFET, Y. 2013. Variable-depth streamer acquisition: Broadband data for imaging and inversion. *Society of Exploration Geophysicists*, 78 13.

URICK, R. J. 1979. *Sound propagation in the sea,* Washington D.C 20046, The Catholic University of America.

WAN, L. 2010. *MATCHED FIELD PROCESSING BASED GEO-ACOUSTIC INVERSION IN SHALLOW WATER.* PHD In Partial Fulfillment of the Requirements for the Degree Doctor of Philosophy in the School of Mechanical Engineering, Georgia Institute of Technology.

WESTON, D. E. 1959. A Moire Fringe Analog of Sound Propagation in Shallow Water. 32**,** 8.

WILSON, W. D. 1960. Equation for the speed of sound in sea water. 32.

YANG, J. 2007. *SPATIAL COHERENCE IN A SHALLOW WATER WAVEGUIDE.* Doctoral of Philosophy In Partial Fulfillment of the Requirements for the Degree Doctoral of Philosophy, Georgia Institute of Technology.

ZHANG, Z. & TINDLE, C. 1993a. Complex effective depth of the ocean bottom. *The Journal of the Acoustical Society of America,* 93**,** 205-213.

ZHANG, Z. Y. & TINDLE, C. T. 1993b. Complex effective depth of the ocean bottom. *Journal of the Acoustical Society of America,* 93**,** 9.

8. Appendices

Appendix A: Velocity-pressure relation for plane-wave solutions

According to (Ross, 1987) for a moving water particle in a certain direction (+x), then the net pressure in the +x-direction acting on the fluid particle is given as:

$$net\ pressure = -\left(\frac{\partial p}{\partial x}\right)\Delta x \qquad \text{(A1)}$$

$$The\ net\ force\ F = -\left(\frac{\partial p}{\partial x}\right)\Delta x\Delta y\Delta z \qquad \text{(A2)}$$

Mass of the particle $m = density \times volume = \rho\Delta x\Delta y\Delta z$

From Newton's law of motion: $The\ net\ force\ F = mass \times acceleration = ma, and\ a = \frac{\partial u}{\partial t}$

$$-\left(\frac{\partial p}{\partial x}\right)\Delta x\Delta y\Delta z = \rho\Delta x\Delta y\Delta z\frac{\partial u}{\partial t} \qquad \text{(A3)}$$

$$-\left(\frac{\partial p}{\partial x}\right) = \rho\frac{\partial u}{\partial t} \qquad \text{(A4)}$$

A wave traveling in the +x-direction has particle velocity component $u = u(x - ct)$ and therefore

$$\frac{\partial u}{\partial t} = -c\frac{\partial u}{\partial x} \qquad \text{(A5)}$$

Then substituting equation (A5) in equation (A4) yields

$$\frac{\partial p}{\partial x} = \rho c\frac{\partial u}{\partial x} \qquad \text{(A6)}$$

Integrating both sides we get for the case of a plane-wave of sound, that acoustic pressure (p) is related to the particle velocity (u) by:

$$p = \pm(\rho c)u \qquad \text{(A7)}$$

where $\pm$ sign is indicates a wave traveling either in the positive (+) or negative (-) -x-direction and the term ρc is called the specific acoustic resistance and its value in sea water is 1.5×10^5 g/cm^{2}s and for air is 42 g/cm^{2}s.

Appendix B: Values of constants in the François and Garrison's empirical formula for the attenuation in sea water

Ross (1987) introduced, based on earlier results of François and Garrison (1982), the empirical formula for the attenuation in sea water as the sum of two relaxation terms and a viscosity component (Medwin and Clay, 1998):

$$\alpha = \frac{A_1 P_1 f_1 f^2}{f^2 + f_1^2} + \frac{A_2 P_2 f_2 f^2}{f^2 + f_2^2} + A_3 P_3 f^2 \qquad (B1)$$

where α is the absorption coefficient in dB/km. The coefficients are expressed in terms of z = depth (m); T = Temperature (℃); S = salinity (parts/1000); and the relaxation frequencies f_1 for Boric acid and f_2 for Magnesium sulfate. The constants are:

Boric acid component in sea water

$$A_1 = \frac{8.68}{c} 10^{(0.78pH-5)}\, dB/km/kHz \qquad (B2)$$

$$\boldsymbol{p_1 = 1,}$$

$$f_1 = 2.8\left(\frac{s}{35}\right)^{0.5} 10^{(4-1245/(273+T))}\, kHz \qquad (B2)$$

Magnesium sulfate component in sea water

$$A_2 = 21.44\left(\frac{S}{c}\right)(1 + 0.025T) dB/km/kHz \qquad (B3)$$

$$p_2 = 1 - 1.37 \times 10^{-4} z + 6.2 \times 10^{-9} z^2 \qquad (B4)$$

$$f_2 = \frac{8.17 \times 10^{[8-1990/(273+T)]}}{1 + 0.0018(S-35)}\, kHz \qquad (B5)$$

Pure water (shear viscosity) component for $T \leq 20$℃

$$A_3 = 4.937 \times 10^{-4} - 2.59 \times 10^{-5} T + 9.11 \times 10^{-7} T^2 -$$

$$1.5 \times 10^{-8} T^3 \; dB/km/kHz^2 \tag{B6}$$

For $T \leq 20℃$

$$A_3 = 3.964 \times 10^{-4} - 1.146 \times 10^{-5} T + 1.45 \times 10^{-7} T^2 - 6.5 \times 10^{-8} T^3 \; dB/km/kHz^2 \tag{B7}$$

$$p_3 = 1 - 1.383 \times 10^{-5} z + 4.9 \times 10^{-10} z^2 \tag{B8}$$

However a simplified expression for the frequency dependence ($f \; in \; kHz$) of the attenuation (α) in sea water was expressed by Jensen et al. (1994) is:

$$\alpha \approx 3.3 \times 10^{-3} + \frac{0.11 f^2}{4100 + f^2} + 3 \times 10^{-4} f^2 \tag{B9}$$

Appendix C : Effective depth approximation

From fig.4.1 we see that the ray segments s and s ' in the figure are given by the trigonometric relation:

$$s = \frac{\Delta H}{sin\theta} \quad and \quad s' = 2scos^2\theta = \frac{2\Delta H cos^2\theta}{sin\theta} \tag{C1}$$

Relative to the phase of the incident wave at the boundary, the phase of the reflected plane wave at points A and B is given by

$$\Phi_A = k_w s' + \psi(\theta) \quad and \; \Phi_B = 2k_w s + \psi' \tag{C2}$$

where $k_w = k = \frac{\omega}{c_1}$. For A and B to lie on the same wave front then, $\Phi_A = \Phi_B$ and after substitution we get

$$\left.\begin{aligned} \psi(\theta) - \psi' &= 2k_w s - k_w s' \\ \psi(\theta) - \psi' &= k_w (2\frac{\Delta H}{sin\theta} - \frac{2\Delta H cos^2\theta}{sin\theta}) \\ \psi(\theta) - \psi' &= \frac{2k_w \Delta H}{sin\theta}(1 - cos^2\theta) \\ \psi(\theta) - \psi' &= 2k_w \Delta H sin\theta \\ \Delta H(\theta) &= \frac{\psi(\theta) - \psi'}{2k_w sin\theta} \end{aligned}\right\} \tag{C3}$$

Appendix D: The speed of sound in sea water

The speed of sound in sea water depends on its temperature, as well as on the salinity and hydrostatic pressure. For calculation of the speed of sound, Wilson's empirical formula is of common use (Wilson, 1960), and accepted by the National Oceanographic Data Center (NODC), USA, for computer processing of hydrological information.

Wilson's formula can be expressed as follows

$$c(S,T,P) = c_0 + \Delta c_T + \Delta c_S + \Delta c_P + \Delta c_{STP} \quad \text{(D1)}$$

where

$$\left.\begin{aligned} c_0 &= 1449.14\,, \\ \Delta c_T &= 4.5721T - 4.4532\times10^{-2}\,T^2 - 2.6045\times10^{-4}\,T^3 + 7.9851\times10^{-6}\,T^4, \\ \Delta c_S &= 1.39799(S-35) - 1.69202\times10^{-3}(S-35)^2, \\ \Delta c_P &= 1.63432P - 1.06768\times10^{-3}P^2 + 3.73403\times10^{-6}P^3 - 3.6332\times10^{-8}P^4, \\ \Delta c_{STP} &= (S-35)(-1.1244\times10^{-2}T + 7.7711\times10^{-7}T^2 + 7.85344\times10^{-4}P \\ &\quad - 1.3458\times10^{-5}P^2 + 3.2203\times10^{-7}PT + 1.6101\times10^{-8}T^2P) \\ &\quad + P(-1.8974\times10^{-3}T + 7.6287\times10^{-5}T^2 + 4.6176\times10^{-7}T^3) \\ &\quad + P^2(-2.6301\times10^{-5}T + 1.9302\times10^{-7}T^2) + P^3(-2.0831\times10^{-7}T) \end{aligned}\right\} \quad \text{(D2)}$$

with c(S,T,P) is speed of sound, m/s; T is temperature, °C; S is salinity, (parts/1000) and P is hydrostatic pressure, MPa

Appendix E: Matlab code for Pekeris waveguide

Simulations of propagation of sound wave in Pekeris waveguide model

```
% NOISE [p(r,Z)] = NOISE(P(r,Z))
% Purpose: simulate propagation of sound wave in Pekeris
waveguide model

% Parameters:
% c1 = sound speed in ocean channel [1500 m/s]
% c2 = sound speed in bottom medium [1600 m/s]
% rho1 = density of water [1000 kg/m^3]
% rho 2 = density of bottom medium [1250 kg/m^3]
% rho    = density ratio [rho = rho2/rho1 = 1.25]
```

```
% H = depth of ocean channel [54 m]
% r = propagation distance (offset)
% n = mode number (default = first [n = 1])
%f = frequency
%k = horizontal wave number
%gamma = vertical wave number
% omega = angular frequency [omega = 2*pi*f]
%alphas = S wave attenuation factor in second layer
%alpha2 = attenuation factor in second layer
% Author: Deneke Admasu Fetene, Univ. of Oslo, Dept. of Geo.
Scinces
% June 5, 2014.


H      = 54;                          % Thickness of layer
c1     = 1500;                        % Vp of water layer
c2     = 1600;                        % Vp of second layer
cs     = 0;                           % Vs of second layer
rho    = 1.25;                        % rho = rho2/rho1
rho1   = 1000;                        % density of water
rho2   = rho*rho1;                    % density of bottom medium
alphas = 0;                           % S wave attenuation factor
in second layer
f      = 100;                         % frequency [100 Hz]
omega = 2*pi*f;                       % angular frequency
alpha2 = 0.003597789207803; %attenuation factor in 2nd layer
%alpha2 = 0.3125dB/m/kHz;

nitr = 400;                           % Number of iteration
Nmax = 4;                             % maximum mode number
r    = linspace(0.1,4.5e3,1001);      % offset[m]
Zs   = 9;                             % source depth
Zr   = 10.8;                          % receiver depth
aa   = (sqrt((2*pi)./r)).*(exp((1i*pi)./4));

for n = 1:Nmax

    kw     = (omega/c1);
    cscw   = cs/c1;
    theta  = 0.15*pi/180;
    k      = (omega/c1)*cos (theta); % initial k

    for ii = 1:nitr

        gamma = sqrt(((omega/c1)^2)-k^2);
        omatp = (omega/c2) + 1i*alpha2;
        omats = (omega/cs) + 1i*alphas;
        etta  = sqrt(k^2 - omatp^2);
        betta = sqrt(omats^2 - k^2);
        P = 1;
```

```
 P     = (1 - (2*k^2)/(omats^2))^2 +
(1i*4*etta*betta*k^2)/((omats)^4);
        P(isnan(P)) = 1;

        A =((1-
((2*k^2)./(omats^2)))^2)+((8*etta^2)./(omats^2)).*(1-
((2*k^2)./(omats^2)))-((1i*4*etta^3)./betta*(omats^2)).*(2-
((3*k^2)./(omats^2)));
        %A = 1;
        A(isnan(A)) = 1;
        num   = rho2*gamma*P - 1i*rho1*etta;
        den   = rho2*gamma*P + 1i*rho1*etta;
        V     = num/den;
        phi   = -1i*log(V);
        delH  = (phi + pi)/(2*gamma);

        He    = H + delH; % effective depth
        gamma = (n*pi)/He;

        kn = sqrt((omega/c1)^2 - gamma^2);
        if (abs(k-kn)<0.0001)
            break;
        end
        theta = asin(gamma/kw);
        k = kn;

    end

    Q        = (H/2) -
(sin(2*gamma*H)/4*gamma)+((1/rho)*((sin(gamma*H)^2)/2*etta)).*
(A/P^2);

 if(imag(kn) < 0)
        break
    end

    gg       =
(1/Q).*sin(gamma*Zs).*sin(gamma*Zr).*(sqrt(1/kn));
    po(n,:)  = gg.*exp(1i*kn*r);
    qo(n,:)  = gg.*exp(1i*kn*r);
end

PP = aa.*sum(po,1);
PPP = abs(PP)./abs(PP(1));

figure; plot(r,mag2db(abs(PPP)), 'b');grid on;
xlabel('Range (m)')
ylabel('Loss(dB re 1m)')
ylim([-80 -30])
title('Propagation loss as a function of range for a Pekeris
waveguide, mode 4')
```